JAMES | Journal of Advances in Modeling Earth Systems

RESEARCH ARTICLE
10.1029/2021MS002791

Key Points:

- The number of spontaneously generated tropical cyclones (TCs) in a free-running general circulation model (GCM) can be controlled by physics timestep
- In the Community Atmosphere Model, shorter timesteps promote higher TC frequencies due to upscale growth of near-grid scale processes
- Tropical cyclones frequencies at shorter timesteps can be reduced by increasing the amount of instability removed by the convective parameterization

Correspondence to:
C. M. Zarzycki,
cmz5202@psu.edu

Citation:
Zarzycki, C. M. (2022). Sowing storms: How model timestep can control tropical cyclone frequency in a GCM. *Journal of Advances in Modeling Earth Systems*, *14*, e2021MS002791. https://doi.org/10.1029/2021MS002791

Received 22 AUG 2021
Accepted 14 FEB 2022

Sowing Storms: How Model Timestep Can Control Tropical Cyclone Frequency in a GCM

Colin M. Zarzycki[1]

[1]Pennsylvania State University, University Park, PA, USA

Abstract With general circulation models (GCMs) being increasingly used to explore extreme events over short temporal and small spatial scales, understanding how design choices in model configuration impact simulation results is critical. This research shows that the number of spontaneously generated tropical cyclones (TCs) in a version of the Community Atmosphere Model can be controlled by changing the coupling frequency between the dynamical core and physical parameterizations. More frequent coupling (i.e., shorter physics timesteps), even in the presence of an otherwise identical model, leads to large increases in TC activity. It is suggested that this arises due to competition within moist physics subroutines. Simulations with reduced physics timesteps preferentially eliminate instantaneous atmospheric instability via grid-scale motions, even while producing mean climates similar to those with longer timesteps. These small-scale variability increases lead to more tropical "seeds," which are converted to full-fledged TCs. This behavior is confirmed through a set of sensitivity experiments and highlights the caution needed in studying and generalizing phenomena that depend on both resolved and sub-grid scales in GCMs and the need for targeting physics-dynamics coupling as a model improvement strategy.

Plain Language Summary Before an atmospheric model can produce data to be analyzed, a scientist must make a multitude of choices controlling subtle aspects of how the model runs. One such design choice is the "model timestep," or, how big the time increments are as the model marches forward in time. This work shows that the number of tropical cyclones in climate data is sensitive to this step size. As the step size is made smaller, the number of cyclones goes up, even if every other piece of the model code is kept identical. This occurs because changes in the timestep affect the amount of precipitation generated by different parts of the model and at which spatial scales it falls over.

1. Introduction

General circulation models (GCMs) are a tool of choice for scientists and stakeholders alike. GCMs consist of two primary components; the dynamical core and the subgrid parameterization suite (i.e., the physics package). The dynamical core is the component responsible for simulating resolved fluid flow by solving the Navier-Stokes equations. The subgrid parameterizations, on the other hand, handle unresolved processes that occur at the subgrid scale. For the foreseeable future, both are necessary for proper simulation of the Earth system. Design choices in these components (e.g., numerical methods, parameter values, etc.) play a key role in the climate simulated by GCMs, although this area is under-researched when compared to the volume of work exploring simulated climates themselves.

One such design choice is model timestep (dt). Many GCMs apply different timesteps for the dynamical core and parameterization suite, with dt_{dyn} generally being constrained by the Courant-Friedrichs-Lewy (CFL) stability condition. Conversely, while exceedingly long physics timesteps can produce undesirable artifacts (e.g., Teixeira et al. (2007); Thatcher and Jablonowski (2016)), GCMs are typically stable with longer dt_{phys}. This difference in dt_{dyn} and dt_{phys} required for numerical stability leads to the common approach of sub-cycling the dynamics and taking a longer physics timestep in order to reduce the computational burden associated with model simulations (Hourdin et al., 2017) and decrease time-to-solution (Beljaars et al., 2018).

In addition to timestep, another design choice that impacts the behavior of GCMs is how tendencies from different components within the subgrid parameterization suite are combined. There are two types of splitting commonly used in GCMs: parallel (or process) splitting, where all parameterization components start from the same state and their tendencies are summed at the end of a timestep, and sequential (or time) splitting, where parameterizations

are called in a particular order and each subsequent parameterization utilizes updates to the state from previous parameterizations already applied at that timestep (Donahue & Caldwell, 2020; Williamson, 2002).

The timestep choice and the mechanics of how the dynamical core and subgrid parameterizations communicate with one another fall under the broad umbrella of "physics-dynamics coupling (PDC)." The impact of PDC and timestepping errors has been even more infrequently studied, at least compared to spatial discretizations, resolution, parameterizations, and other more commonly discussed design choices. A comprehensive review of recent challenges associated with PDC can be found in Gross et al. (2018).

PDC errors, while difficult to isolate, can impact climate substantially. Beljaars et al. (2004) showed non-negligible differences when comparing numerical weather prediction forecasts with a 10-min timestep versus a 5-min one (see also Beljaars et al. (2018)). Williamson and Olson (2003) found that aquaplanet simulations could exhibit either a single or dual peak in the intertropical convergence zone (ITCZ), in part due to how much convective available potential energy (CAPE) could accumulate between subsequent timesteps of differing length. Mishra and Sahany (2011) noted changes in the partitioning between resolved and convective precipitation due to varying timesteps in a low-resolution version of the Community Atmosphere Model, version 3 (CAM3). Williamson (2013) hypothesized that the competition for the consumption of CAPE between explicit stratiform condensation and parameterized convection was altered with shorter model timesteps, leading to fundamental changes in simulated precipitation. Wan et al. (2014) found that reductions in timestep in CAM resulted in corresponding increases in resolved precipitation as well as both liquid and ice water paths. Herrington and Reed (2018) argued that long physics timesteps in idealized simulations exacerbated time truncation errors and resulted in a decoupling of analytic relationships between grid spacing and resolved vertical motions. Both Wan et al. (2021) and Santos et al. (2021) found large changes in cloud properties when a variety of timesteps were changed in the E3SM Atmospheric Model, including the physics timestep itself and the sub-cycling of various moist processes within the physics package. Even in superparameterized (Yu & Pritchard, 2015) and convective-permitting (Barrett et al., 2019) simulations, timestep sensitivity has been noted in the simulation of clouds and precipitation.

As model grid spacings grow smaller, extreme weather events—important targets for research given their outsized societal impacts—are better simulated due to improved resolution. In higher resolution GCMs, the interaction between resolved and parameterized convection becomes particularly complex. The "gray zone" is defined as a range of grid resolutions where convective plumes are partially resolved but a convective parameterization is still needed to account for small scale processes (Arakawa, 2004; Frank, 1983). At higher resolution, the general assumption has been that the physics timestep should be smaller, owing to the fact that the timescales associated with atmospheric motion are correlated to their spatial scale (Smagorinsky, 1974). Therefore, smaller parameterization timesteps are needed to ensure subgrid processes are evaluated at timescales appropriate to small-scale phenomena, such as convection.

An extreme phenomena of interest is the tropical cyclone (TC). TCs are intense storms originating in tropical ocean basins characterized by their strong surface winds, heavy rain, high waves, and damaging storm surge. They are estimated to be responsible for 19,000 fatalities and $26 billion (USD) in global damages annually (Mendelsohn et al., 2012), making them one of the most devastating natural phenomena and an important target for modelers. Previous work has shown that TC simulation in GCMs can be sensitive to configuration, including dynamical core choice (Guimond et al., 2016; Reed et al., 2015; Zhao et al., 2012), physical parameterizations (Kim et al., 2012; Lim et al., 2015; Reed & Jablonowski, 2011; Vitart et al., 2001; X. Li et al., 2020), and ocean coupling strategy (H. Li & Sriver, 2018; Scoccimarro et al., 2017; Zarzycki, 2016; Zarzycki et al., 2016). While the influences of some model design choices on TCs have been explored, formally contextualizing how actionable climate data is impacted by such decisions remains sparsely researched.

There has also been little investigation into the role of PDC and timestepping in GCM-simulated TCs. Reed et al. (2012) found that idealized TCs at 0.25° resolution increased in intensity with decreasing timestep, which they attributed to increased resolved-scale precipitation. Similarly, X. Li et al. (2020) explored the sensitivity of TCs in both 1° and 0.25° versions of CAM to model timestep. Like Reed et al. (2012), their study focused on changes in storm structure using a conditional approach (i.e., the model is initialized with an existing TC vortex) and found that TC intensity generally decreased (increased) with decreasing timestep at 1° (0.25°) grid spacing.

In this paper, a sensitivity at the physics-dynamics interface that manifests in changes in the number of spontaneously generated TCs in a GCM with differing physics timesteps is described. While previous work in this area has generally focused on mean climate response, large impacts on storm-level data are demonstrated here. Bit-for-bit identical code (i.e., identical dynamical core and parameterizations) can lead to extremely different simulated storm statistics by modifying the frequency at which the physics and dynamics are coupled to one another. This work is also unique in that it is not conditional on the existence of an initialized TC and permits the model to generate its own internal storm climatology.

2. Methods

2.1. Model

In this study, we apply an updated version of the Community Atmosphere Model version 5 (CAM5) (Neale et al., 2012), with the variable-resolution (V-R) option (Zarzycki et al., 2014) of the spectral-element (CAM-SE) dynamical core (Dennis et al., 2012; Taylor et al., 2007). CAM5 is the atmospheric component of the Community Earth System Model (CESM) version 1.2 (Hurrell et al., 2013). The configuration here closely mirrors the release version of CAM5 in CESM1.2. The two primary differences are a newer version of the Morrison-Gettelman microphysics (MG2, Gettelman and Morrison (2015)) and that CAM is coupled to the newest version of the Community Land Model, version 5 (CLM5, Lawrence et al. (2019)).

In CAM5, the timestep for the dynamical core (dt_{dyn}) is different from the parameterization suite and component coupling (dt_{phys}). The specifics for the SE dynamical core timestepping are outlined in Lauritzen et al. (2018), but most relevant here is that the dynamics timestep depends on the CFL criterion and is halved when grid spacing is halved to maintain numerical stability (e.g., dt_{dyn} is 90s (360s) for 0.25° (1°) grid spacing).

Conversely, dt_{phys} is longer due to less restrictive numerical stability requirements. In CAM5-SE, the default dt_{phys} is 1800s (900s) compared to a default dt_{dyn} of 360s (90s) for 1° (0.25°) simulations (Lauritzen et al., 2018). The dynamics is therefore "substepped" or "subcycled." For example, with a dt_{phys} of 900s and a dt_{dyn} of 90s, 10 dynamics timesteps take place between calls to the physics package. This technique is applied to reduce the computational cost of climate models, particularly when the parameterization suite is expensive, as it is in CAM5. Since the timescale at which the resolved atmosphere is updated with tendencies from the physical parameterizations is governed by dt_{phys}, this is also referred to as the "coupling interval" or "coupling frequency."

2.1.1. Deep Convection, Large-Scale Microphysics, and Process Ordering in CAM5

Because CAM5 is a hydrostatic model run at grid spacings coarser than 10 km, it requires convective parameterization. In particular, the Zhang-McFarlane (ZM) deep convective parameterization (Zhang & McFarlane, 1995) is used in CAM5. A full description of the scheme as implemented is contained in Neale et al. (2012). Here we only highlight aspects of the parameterization relevant to this study.

ZM is based on a plume ensemble approach where an ensemble of subgrid updrafts exists within a particular grid cell when the atmosphere is defined to be conditionally unstable in the column (Zhang & McFarlane, 1995). Moist convection occurs when sufficient CAPE exists and as parcels ascend. CAPE within cumulus clouds (A) is consumed according to the following relationship:

$$\frac{\partial A}{\partial t} = -M_b F \tag{1}$$

where M_b is the cloud base upward mass flux and F is the CAPE consumed per unit cloud base updraft mass flux. To close the formulation, the following relationship is used:

$$F = \frac{A}{\tau M_b} \tag{2}$$

where τ is a characteristic time scale. If we assume M_b and F are constant over a model parameterization timestep dt_{phys}, combining the above gives:

$$A = A_0 \left(1 - dt_{phys}/\tau\right) \tag{3}$$

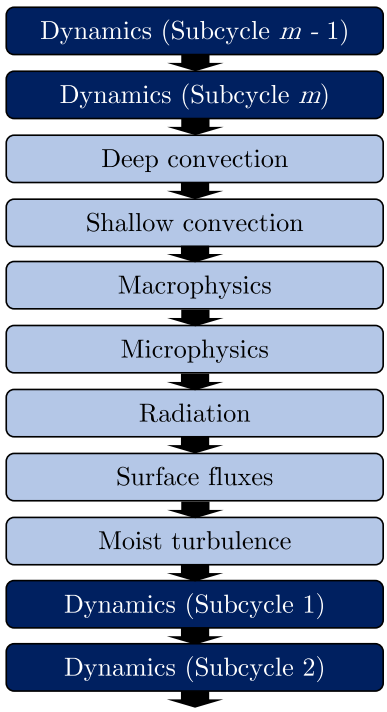

Figure 1. Flowchart for sequential-splitting of major parameterizations within the Community Atmosphere Model version 5. Boxes in light blue are part of the subgrid physics package while dark blue denotes the dynamical core. The number of subcycled steps in the dynamical core (m) for a given resolution is equal to dt_{phys}/dt_{dyn}. Note that this is not an exhaustive list and some processes are omitted for brevity. Loosely based on Figure 1 in Park et al. (2014).

where A_0 and A are CAPE before and after the parameterization are applied, respectively. τ is defined to be a hardcoded constant in CAM and is set to a value of 3600s. CAM5 also includes a shallow convective parameterization (Park & Bretherton, 2009). Here, we refer to "convective" precipitation as the sum of that produced by both deep and shallow schemes, although in the domains and phenomena considered in this study, physics tendencies overwhelmingly come from ZM, therefore we will assume that changes in subgrid convection are dominated by the ZM scheme.

Large-scale condensation is handled within the stratiform parameterization set, and serves to bring any remaining supersaturation within the column back to saturation. While technically two distinct subroutines, stratiform macrophysics and microphysics are tightly intertwined with one another, with macrophysics handling the conversion of vapor to liquid and microphysics defining the distribution of droplets/particles, mass fraction between liquid and ice, and eventual precipitation at the surface (Gettelman et al., 2010; Morrison & Gettelman, 2008). These parameterizations act on the model state and do not directly adjust the stability of the column (although they provide thermodynamic updates to the dynamics). Because of this, we refer to these simply as "large-scale" or "resolved-scale" parameterizations and treat them as providing a hard adjustment to a supersaturated atmosphere (i.e., in the presence of an unstable profile, a column-scale stabilization overturning occurs within the dynamics which results in supersaturation and resultant precipitation in a single timestep).

Within the CAM physics suite, parameterizations are sequentially split, which means each subsequent parameterization starts from the state updated by the preceding parameterization and all components are called in this sequential fashion (Williamson, 2002). Of particular importance here, the deep convective parameterization (ZM) is called prior to the resolved-scale microphysics (MG2) in the parameterization sequence for a given timestep. A thorough analysis of the order in which parameterizations are applied as a design choice can be found in Donahue and Caldwell (2018), here we only consider the ordering applied in the public release of the model. A simple schematic of this process ordering is shown in Figure 1.

2.2. Experimental Configurations

We complete an ensemble of simulations using CAM5 with identical source code. All tuning parameters are left as default values in the public release version unless otherwise stated. All simulations follow Atmospheric Model Intercomparison Project (AMIP, Gates et al. (1999)) protocols. Temporally-evolving historical sea surface temperatures (SSTs) and sea ice are specified and applied as boundary conditions via the HadSST (Hurrell et al., 2008) data set. It should be noted that specified SSTs provide one-way coupling and do not permit TC cold wakes nor their associated surface enthalpy flux negative feedback (Zarzycki, 2016). Given even high-resolution global models partially under-resolve TC structure (Davis, 2018) and coupled models suffer from mean SST biases that can impact TC climatology (Roberts et al., 2020), this is an appropriate approximation, particularly since we are interested in the relative difference between simulations. Greenhouse gas concentrations and aerosol climatology are prescribed to reproduce observations. The model is initialized in 1984 with the first year removed from each analysis to ensure representative internal climatologies.

To reduce computational requirements, a V-R mesh centered over the North Atlantic Ocean (NATL) is applied. This mesh is shown in Figure 2 and has been used in previous regional TC studies with CAM-SE (Reed et al., 2020; Stansfield, Reed, & Zarzycki, 2020; Stansfield, Reed, Zarzycki, Ullrich, & Chavas, 2020; Zarzycki et al., 2017), with simulated climatologies described therein. V-R grids in CAM-SE have been shown to reproduce regional statistics when compared to globally-uniform high-resolution meshes at a cost that scales approximately linearly with the reduced number of elements (Zarzycki et al., 2014). Here, the refined mesh over the NATL is approximately 0.25° (28 km), which is considered the "high-resolution" configuration of

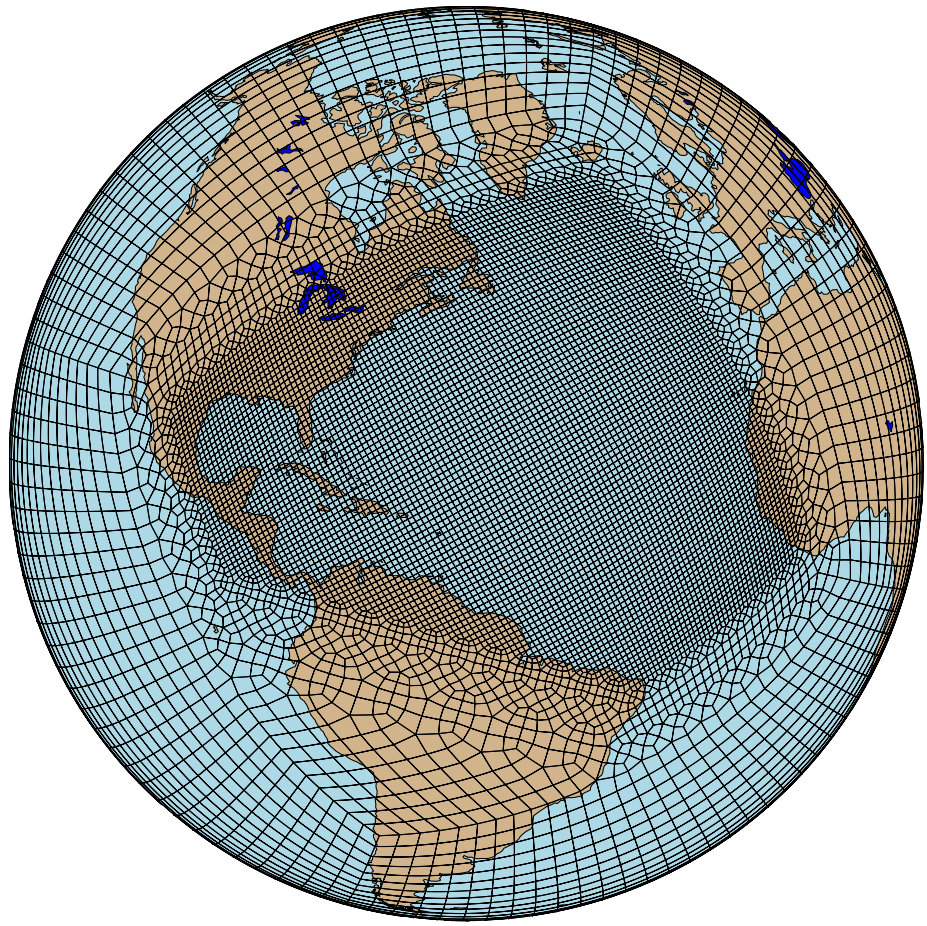

Figure 2. Variable-resolution Community Atmosphere Model-spectral element grid used in this study. The innermost nest over the North Atlantic Basin is nominally 0.25° (28 km) grid spacing.

CAM used for previous studies (Bacmeister et al., 2014; Roberts et al., 2020; Walsh et al., 2015; Wehner et al., 2014). The background global grid is 1°. All model components (e.g., atmosphere, land, ocean, etc.) use the same grid, eliminating the need for spatial remapping during coupling. Explicit diffusion is scaled by adjusting a scalar hyperdiffusion coefficient based on local grid spacing as defined in Zarzycki et al. (2014). While physics tendencies are only calculated every dt_{phys}, we apply them fractionally at every dynamics substep (i.e., se_type = 0 in CAM-SE) as in Thatcher and Jablonowski (2016), who showed this method reduced undesirable large-scale gravity waves excited by long dt_{phys}.

Table 1
Experimental Details in This Paper

Name	Years	dt_{dyn}	dt_{phys} (ATM_NCPL)	τ	dmpdz
dt_{1800}	22	90s	1800s (48)	3600s	1×10^{-3}
dt_{900}	22	90s	900s (92)	3600s	1×10^{-3}
dt_{450}	22	90s	450s (192)	3600s	1×10^{-3}
$dt_{450,\tau-}$	22	90s	450s (192)	900s	1×10^{-3}
$dt_{450,dmpdz}$	22	90s	450s (192)	3600s	0.3×10^{-3}

Note. dt_{dyn} is the dynamics timestep, dt_{phys} is the physics timestep (governed in CAM by the number of physics-dynamics coupling calls per day, ATM_NCPL), τ is the convective timescale in Zhang-McFarlane (ZM), and *dmpdz* is the entrainment factor in ZM. The top three are considered the base experiments, while the latter two are discussed in the sensitivity section.

Five simulations are completed, shown in Table 1. The dynamics timestep (dt_{dyn}) is the same in all simulations since it is governed by the finest grid spacing to satisfy the CFL criterion. Three simulations hold τ fixed at 3600s, which is the default value in ZM. The only change distinguishing these three simulations is to dt_{phys}, governed by setting a single variable (ATM_NCPL) in the CAM configuration at model run time. Two sensitivity simulations hold dt_{phys} fixed at 450s and contain a single tuning modification to the deep convective parameterization. These will be discussed later in the manuscript.

All analyzed data are 22 years in duration (1985–2006, inclusive). Initial-condition perturbed ensemble members using dt_{900} show similar mean climatologies when compared to one another (Stansfield, Reed, Zarzycki, Ullrich, & Chavas, 2020), therefore the length of these simulations is sufficient to

accurately represent the mean TC climatology of the model. All results are normalized to annual mean values to be comparable with those published by other modeling centers.

2.3. Data Analysis Methodology

To track TCs, we apply the TempestExtremes software package (Ullrich & Zarzycki, 2017; Ullrich et al., 2021). TempestExtremes is a commonly-used and well-vetted tracker for TCs in high-resolution climate data. Briefly, candidate TC centers are flagged by ensuring that a sea level pressure (SLP) minimum is surrounded by a closed contour of SLP 2 hPa greater than the minimum within 5.5°. The geopotential height thickness between the 300 and 500 hPa pressure levels must reach a local maximum to ensure a coherent warm core. This maximum must be spatially-aligned with the SLP minimum (no more than 1° offset in the horizontal) and be encircled by a closed ring of thickness 6 m less than the maximum. Nearby candidates within 6° of one another are merged, with the lowest SLP being kept. Cyclones are then stitched together in time, with storms needing to be equatorward of 50° latitude for at least 60 hr (not necessarily consecutive). Separate trajectories which terminate and begin within 12 hr and 10° of one another are merged to eliminate double-counting of broken tracks. TCs are tracked at standard synoptic reporting times (00Z, 06Z, 12Z, and 18Z). Near-surface wind (u_{10}) is corrected to 10m from the lowest model level winds (approximately 60m) using a logarithmic profile (Garratt, 1992; Wieringa, 1992). The exact mechanics and tunings are explicitly defined in Zarzycki and Ullrich (2017).

Three metrics for a comprehensive evaluation of TC activity are applied. The first is storm count (n), which is just the frequency of discrete trajectories. We also calculate TC Days (TCD) as the total number of days of systems that are flagged as TCs (Webster et al., 2005). Finally, we calculate Accumulated Cyclone Energy (ACE), a further integrated measure that also weights more intense storms more highly than weaker storms (Bell et al., 2000). The inclusion of TCD and ACE provides additional context to cyclone activity beyond absolute numbers, although we generally focus on genesis events in this manuscript. Further details regarding TC metrics in climate models can be found in Zarzycki et al. (2021).

We also broadly quantify TC "seeds." Seeds represent precursor features, generally assumed to be weakly rotating areas in the deep tropics, which may or may not transition to full-fledged TCs depending on a variety of factors including vertical wind shear (DeMaria et al., 2001), midlevel moisture and ventilation (Tang & Emanuel, 2012), and even translation speed (Peng et al., 2012). Since seeds can encompass both developing and non-developing TCs, the number of seeds is often greater than the number of TCs that eventually form, although a single agreed-upon objective metric for precursor features does not exist. Here, we defined seeds as local maxima in the low-level (850 hPa) relative vorticity field ($\zeta_{850} \geq 2.5 \times 10^{-4}\,\mathrm{s}^{-1}$) that originate equatorward of 30° latitude and persist for 12 consecutive hours, similar to Hsieh et al. (2020). We also enforce that seeds must occur during (ASO) to align with the climatological peak of the North Atlantic TC season. Cursory sensitivity analyses showed that increasing (decreasing) the vorticity or duration thresholds or restricting (relaxing) seasonal bounds tracked less (more) TC seeds within the basin, although the relative differences between the model configurations are the same in all cases, demonstrating the findings below are robust to particular seed classification.

Two sets of environmental (large-scale) analyses are performed that include a fixed, large-scale region. Monthly climatologies are derived from the straight average of model output fields. For sub-daily statistics of large-scale fields (e.g., distribution of gridpoint vertical velocities and spectral power of vorticity), we remove the TC itself from output data in order to isolate environments prior to genesis and focus the analysis explicitly on TC frequency controls (e.g., simulations with more TCs will have more extrema in the upward vertical motion fields). This isolation is done by removing all gridpoints within a 5° great-circle radius of a tracked tropical cyclone from the global field before evaluation.

The tropical NATL (or main development region (MDR), Goldenberg and Shapiro (1996)) domain is defined as 5–25°N and 290–345°E and is informed by historical TC genesis climatology. While the TC climatologies are presented for the full calendar year for consistency with previous work, all other analysis specifically focuses on the months of August, September, and October (ASO), as more than 75% of all NATL TCs formed during these three months over the 1980–2019 period. Restricting the TC tracking to ASO provides similar findings.

3. Sensitivity of TCs to Physics Timestep

3.1. TC Frequency

TC track density plots for the three base dt_{phys} configurations are shown in Figure 3. To compare TC climatology, all trajectories at each 6-hourly tracking location are aggregated into 8° × 8° bins over the NATL. Historical observations from the International Best Track Archive for Climate Stewardship (IBTrACS; Knapp et al. (2010)) are shown in the first row for reference (1980–2019). The left column represents the annual average TC track density for each configuration with the difference relative to IBTrACS for that configuration on the right.

As dt_{phys} is reduced from 1800 to 450s (Figures 3b–3d), there is a systematic increase in the number of TCs simulated. CAM5 produces too many TCs for all timesteps over the equator-ward half of the MDR, although this bias is exacerbated with decreasing timestep. More starkly, the dt_{1800} simulation results in too few TCs in the Gulf of Mexico and western half of the NATL basin when compared to historical climatology. The sign of this bias flips as timestep is shortened, with dt_{450} generally producing too many TCs over this region. Interestingly, given this sign change, dt_{900} ends up with the most skillful storm count by virtue of lying between dt_{1800} and dt_{450}.

This is formally corroborated with the annually-averaged, basin-accumulated statistics shown in Table 2. The first line shows the annual reference climatology from IBTrACS (interannual standard deviation in parentheses). The remaining lines list the same statistics for each of the model simulations. The monotonic relationship with dt_{phys} is notable across all three metrics (count, TCD, and ACE). As dt_{phys} is decreased from 1800s to 900s to 450s, the annual frequency (n) of NATL TCs generated by CAM5 increases, with the 450s configuration producing nearly twice as many TCs as the 1800s. This response is also clear in both TCD and ACE. The fact that TCD and ACE follow approximately similar changes with timestep on a relative (i.e., percentage) basis when compared to count implies changes in the frequency of genesis events is the primary driver in this response, not large shifts in storm intensity or lifetime, which would preferentially appear in such metrics. This is also verified by comparing per storm statistics (e.g., average TCD per storm, ACE per storm, etc.), which are broadly similar across the three configurations.

Also shown in Table 2 is the computational cost of each simulation on the National Center for Atmospheric Research's (NCAR's) Cheyenne supercomputer. dt_{450} is 58% more "expensive" than dt_{1800}. Since dt_{dyn} is identical across all simulations, this added cost is due to the increased frequency of calculating subgrid tendencies and the associated coupling. While this is only shown as an informal timing estimate, it further emphasizes the practical motivation of substepping the dynamical core between subsequent calls to the subgrid parameterization suite and why it can be a necessity in the face of computational constraints (e.g., deadline for completing simulations, fixed allocation of resources for a project, etc.).

3.2. Large-Scale Climatology

There are two primary ways dt_{phys} can modulate the atmosphere in order to induce a change in TC frequency. One, the large-scale background state can be modified in a way that makes genesis statistically more probable (i.e., given a fixed number of seeds in an environment, the probability of those becoming full-fledged TCs changes). The second mechanism is through short-term variability within the climate system (i.e., changing the number of seeds themselves, even assuming an unchanged environmental baseline).

We first evaluate the mean climatological state produced by the model during TC season (ASO). The large-scale environment has been shown to be important for statistical prediction of TC genesis events (Camargo et al., 2007). Particular emphasis has been focused on quantities such as SST, atmospheric instability, vertical wind shear, local vorticity, and mid-level relative humidity. Note that for these simulations the SST is prescribed and therefore identical.

Figure 4 shows ASO averages of the tropical NATL for a variety of environmental parameters. The central column is the climatological mean for dt_{900}, with the left (right) columns showing the difference of the dt_{1800} (dt_{450}) simulation relative to dt_{900}. An area weighted mean is also calculated over the MDR, outlined by the black box in each panel and shown in Table 3.

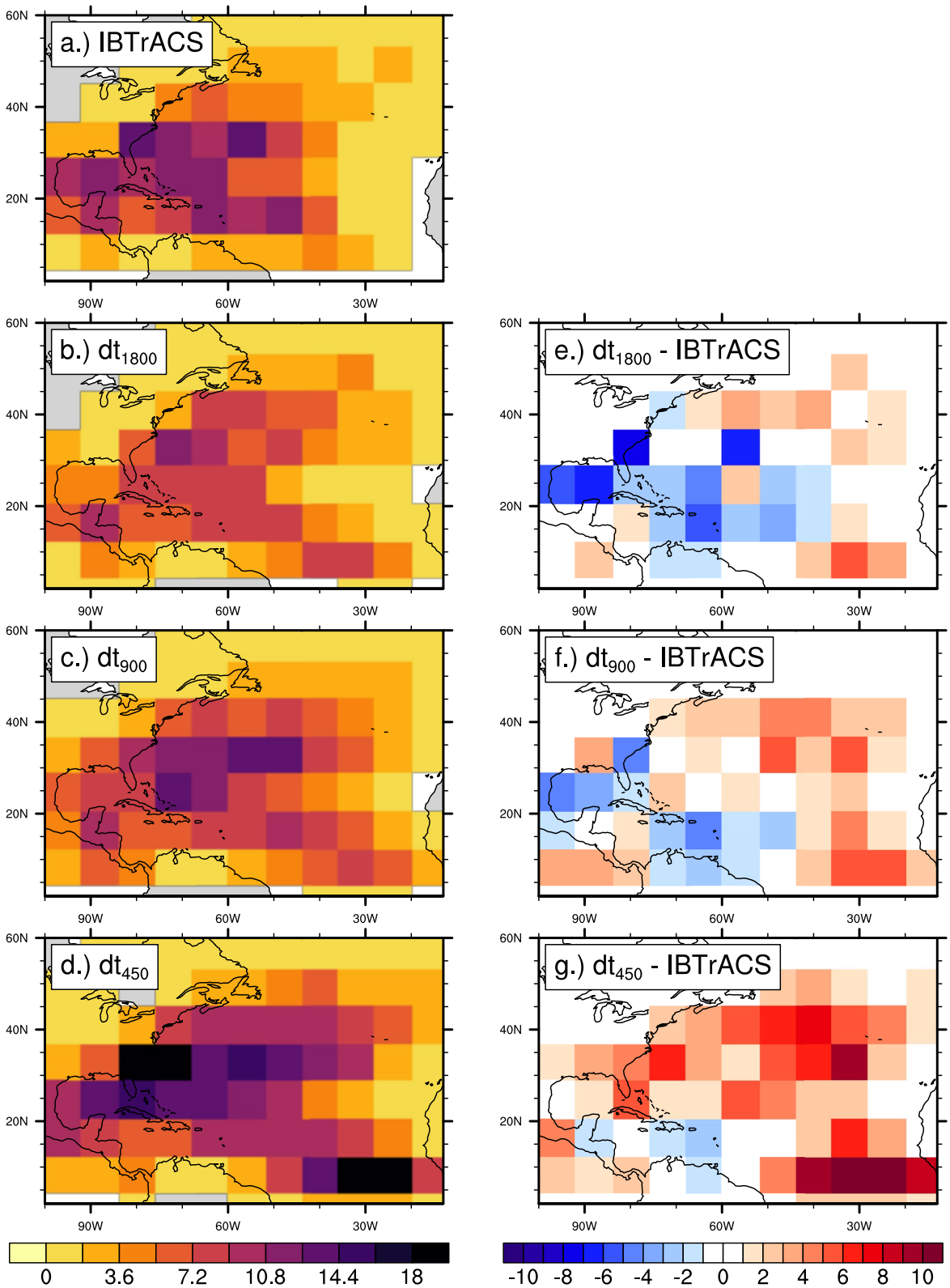

Figure 3. Annually-averaged tropical cyclone (TC) track density for (a) IBTrACS observations and (b–d.) the dt_{1800}, dt_{900}, and dt_{450} simulations. Units are number of TCs transiting per 8° × 8° per year. The bias for each gridbox in the model simulations relative to IBTrACS is shown in (e–h).

Table 2
Mean Annual Tropical Cyclone (TC) Statistics for IBTrACS and the dt_{1800}, dt_{900}, and dt_{450} Simulations

Data	N # yr^{-1}	TCD days yr^{-1}	ACE kn yr^{-1}	Cost CPUh SY^{-1}
IBTrACS	12.3 (5.1)	71.3 (34.7)	121.6 (73.5)	
dt_{1800}	10.6 (3.4)	66.2 (20.6)	62.5 (25.5)	4,310
dt_{900}	13.4 (4.8)	85.9 (37.2)	96.8 (55.5)	5,210
dt_{450}	19.5 (5.4)	125.6 (32.6)	132.2 (60.0)	6,800

Note. *n* Is annual count of TCs over the NATL per year, TCD Is the number of TC days over the NATL per year, and accumulated cyclone energy Is the accumulated cyclone energy over the NATL Per Year. Each column represents one of the three dt_{phys} experiments. The interannual standard deviation for each TC quantity is shown in parentheses. CPUh SY^{-1} = CPU hours (i.e., wall clock time) per simulated year.

The top three rows denote large-scale precipitation, convective precipitation, and total precipitation, which is just the sum of the large-scale and convective components. Convective parameterization dominates the precipitation climatology over the tropical NATL (Figures 4b, 4e and 4h), unsurprising given the ASO timeframe.

Looking at the left and right difference panels, there is notable tradeoff between the large-scale and convective precipitation with changing timestep. As dt_{phys} is shortened (lengthened) the large-scale precipitation increases (decreases) while the convective precipitation decreases (increases). This tradeoff results in somewhat offsetting differences in total precipitation (Figures 4g–4i and third line of Table 3). The 500 hPa pressure velocity (ω_{500}) in Figures 4j–4l is inversely correlated to the total precipitation, implying that areas of increased (decreased) precipitation are associated with more negative (positive) ω_{500} and therefore more (less) upward motion.

In addition to the precipitation and vertical velocity fields, we also evaluate four fields considered to be strong predictors of TC genesis. These are relative vorticity (ζ), moist entropy deficit of the middle troposphere (χ_m), vertical wind shear, and maximum potential intensity (MPI) (Emanuel, 2010). χ_m is calculated at 600 hPa following Emanuel (2013) and MPI is calculated following Bister and Emanuel (2002). These four components are commonly included in genesis potential indices, used to evaluate the conduciveness of a particular regional environment to TC formation (Bruyère et al., 2012; Camargo et al., 2007).

Unlike the precipitation-based quantities, the changes in the mean ASO tropical NATL climatology with model timestep for the genesis variables are relatively small. Neither MPI or wind shear show a monotonic relationship, with highest (lowest) values of MPI (shear) occurring with the intermediate dt_{900}, although all values are within a few percent of one another. χ_m becomes slightly larger as timestep is decreased (from dt_{1800} to dt_{450}), representing a small drying of the middle troposphere. Links between resolved-scale precipitation and subsidence (and associated drying) as a function of model resolution are discussed in Herrington and Reed (2020) and are likely relevant here. Average relative vorticity also decreases slightly as timestep is decreased, indicating a tendency toward more anticyclonic motion in dt_{450}. Interestingly, while this difference is quite small, this response is opposite what might be expected given Table 2, where dt_{450} produced the most TCs.

In general, the key difference between the large-scale climatology of the simulations is the percentage of rainfall that comes from the deep convective parameterization (i.e., the partitioning between resolved and unresolved rainfall). All other quantities (including total precipitation) are within a few percent of one another, implying that the large-scale environment is not sufficiently different between the simulations to explain the large increase in TC activity with decreasing physics timestep.

3.3. Dynamical Processes

While subtle differences exist in the large-scale environmental conditions, these do not appear to be of sufficient magnitude to account for the differences in TC frequency seen in Figure 3 and Table 2. This can be further inferred as the case when noting the required differences in genesis indices to result in an attributable change in TC frequency are large (Camargo et al., 2020). Therefore, if the mean climates are highly similar, TC frequency would need to be impacted by variability on shorter timescales (order of hours to days) within the model. Figure 5 shows the grid-point frequency distribution of three variables in the CAM5 simulations; large-scale precipitation rate (PRECL), convective precipitation rate (PRECC), and 500 hPa vertical pressure velocity (ω_{500}). All variables are instantaneous values within the MDR reported at the same 6-hourly synoptic times used by the TC tracker with TC fields removed using the technique discussed in Section 2.3.

As dt_{phys} decreases, the tails of both the PRECL and ω_{500} distributions are extended toward more extreme values, while the PRECC distribution narrows. The changes in PRECL and PRECC do not offset, resulting in an overall broadening of the precipitation rate distribution with decreasing dt_{phys} (not shown, but can be assumed by combining distributions in Figures 5a and 5b). In GCMs, ω_{500} has been shown to be a good predictor of TC genesis frequency (Zhao & Held, 2012), which would agree with the results in Table 2. The broadening of the

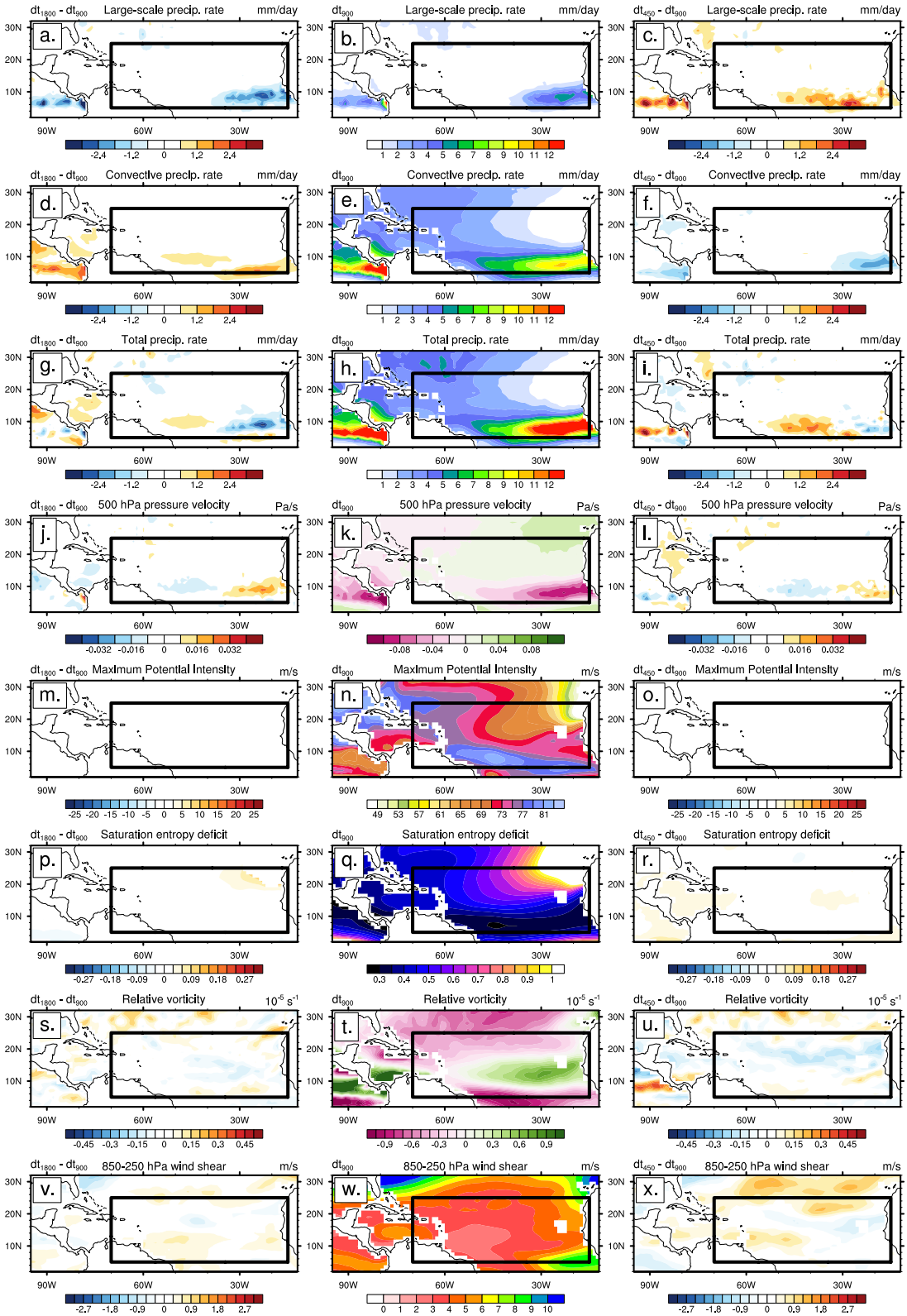

Figure 4. August, September, and October spatial averages of eight quantities important for tropical cyclone genesis. Each row represents a different variable, while each column represents a different model simulation. The central column shows the mean climatology in the dt_{900} simulation, while the left (right) columns show the difference in the dt_{1800} (dt_{450}) climatologies relative to the dt_{900} (center). The Atlantic Main Development Region is outlined in black.

Table 3
August, September, and October Spatial Averages Over the Main Development Region (Black Outlines in Figure 4) for Relevant Large-Scale Variables

Variable	Units	dt_{1800}	dt_{900}	dt_{450}
Large-scale precipitation rate (PRECL)	mm day^{-1}	0.49	0.77	1.05
Convective precipitation rate (PRECC)	mm day^{-1}	3.46	3.29	3.09
Total precipitation rate (PRECT)	mm day^{-1}	3.95	4.06	4.14
Precipitation ratio (PRECL/PRECC)	–	0.14	0.23	0.34
500 hPa pressure velocity (ω_{500})	Pa s^{-1}	-5.43×10^{-3}	-5.66×10^{-3}	-5.69×10^{-3}
Maximum potential intensity (MPI)	m s^{-1}	72.3	72.5	72.3
Saturation entropy deficit (χ_m)	–	0.49	0.49	0.51
Relative vorticity (ζ)	10^5 s^{-1}	−0.13	−0.13	−0.16
850-250 hPa wind shear (VSHEAR)	m s^{-1}	4.24	4.11	4.27

Note. Each column represents one of the three dt_{phys} experiments.

tails with decreasing dt_{phys} in Figures 5b and 5c are consistent with the PRECL and ω_{500} responses noted in the mean climatology in Table 3.

This direct relationship of distribution extremes and TC frequency can be further demonstrated by a simple plot showing the relationship between the 99.9th percentile of 6-hourly instantaneous ASO ω_{500}, PRECC, and PRECL over the MDR versus the number of simulated TCs per year (Figure 6). There is a clear monotonic relationship associated with ω_{500} (PRECL) where objective increases in TC frequency are associated with stronger extremes of upward vertical motion (large-scale precipitation rate) in the tail of the distribution. Also shown is PRECC, which exhibits a far weaker relationship with simulated TCs as a function of timestep. Replacing the x-axis with TCD or ACE results in a similar figure. Given the results in Figures 5 and 6 as well as Table 3, it is obvious that the extreme rainfall rates are dominated by resolved processes and that the decrease in convective precipitation with decreasing dt_{phys} is associated with a broad decrease in the frequency of deep convective precipitation across all rates versus more systematic shifts in the extreme part of the rate distribution.

Figure 7 shows the spectral decomposition of ASO 850 hPa cyclonic relative vorticity (ζ_{850}) over the NATL region. This is done to isolate the background low-level rotation environment, from which TCs can spawn. ζ_{850} at all points within a 5° radius around detected TCs is set to zero. Only cyclonic vorticity (positive in the Northern Hemisphere) is retained, although spectra containing the full relative vorticity field show similar results.

To isolate the refined region of the model important for this study we apply the technique outlined in Errico (1985) to detrend the NATL analysis area in order to apply periodicity to the lateral boundaries. To increase the robustness of the results we average over 960 times (6-hourly instantaneous snapshots for 120 days in two different model years) as in Skamarock (2004) and normalize to power in low-frequency wavenumbers as in Waite (2016).

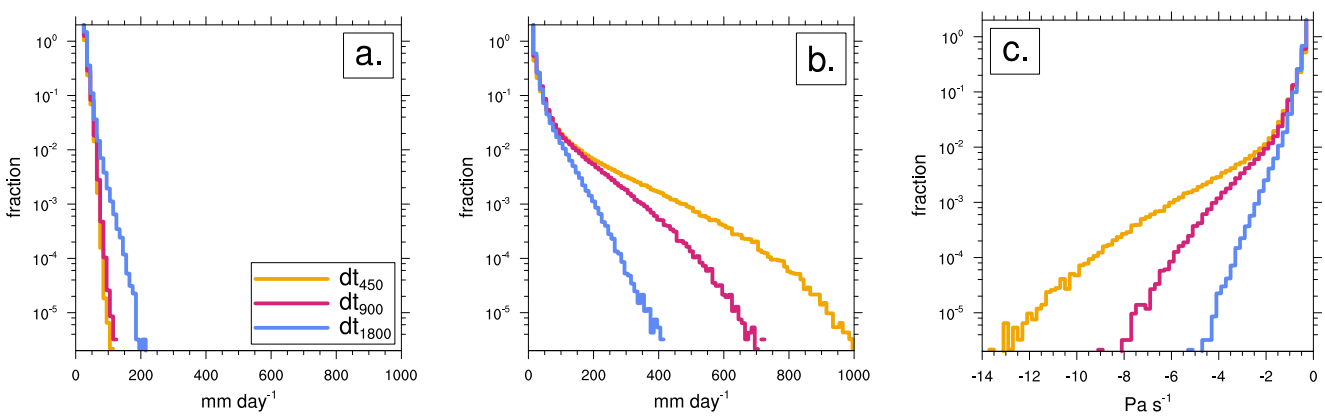

Figure 5. (a) 6-hourly, grid-point, frequency distribution for August, September, and October convective precipitation, (b) large-scale precipitation and (c) 500 hPa vertical pressure velocity over the Main Development Region for the dt_{1800} (blue), dt_{900} (magenta), and dt_{450} (orange) simulations.

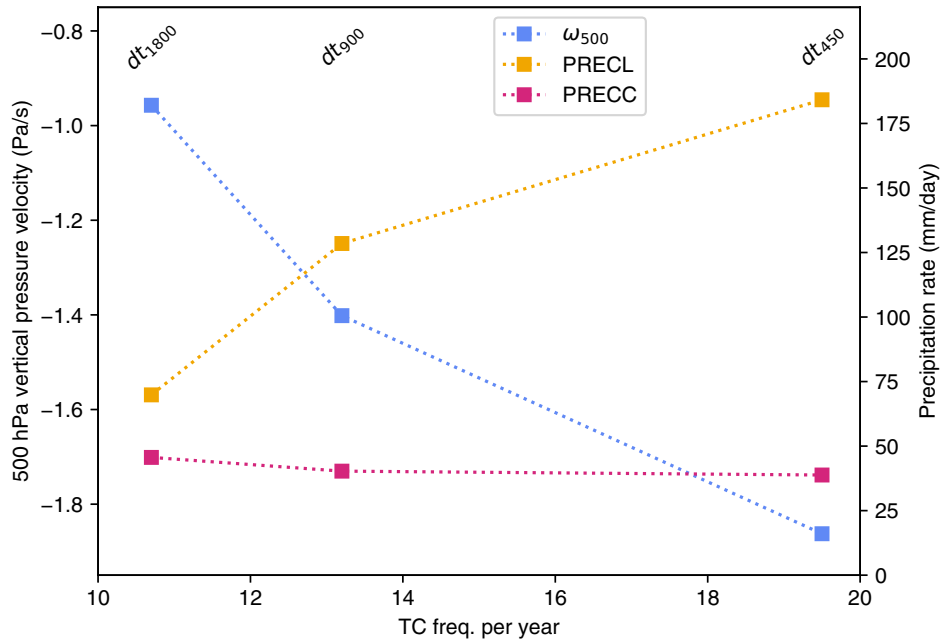

Figure 6. Relationship between annual tropical cyclone frequency (x-axis) and 99.9th percentile of convective precipitation (PRECC, magenta), large-scale precipitation (PRECL, orange) and 500 hPa vertical pressure velocity (ω_{500}, blue) over the Main Development Region for the dt_{1800}, dt_{900}, and dt_{450} simulations.

As dt_{phys} decreases from 1800s to 900s to 450s, there are consistent increases in the power associated with ζ_{850} near the grid scale (far right of distribution). This demonstrates an increase in the near-Δx variance or "noisiness" of the relative vorticity field. In all cases, the increase in small-scale ζ_{850} variance is directly correlated with the TC climatology defined in Section 3.1. It is clear that there is a monotonic relationship between dt_{phys} and ζ_{850} power at the larger wavenumbers on the right side of the plot (small grid sizes). As dt_{phys} is decreased, the power in these near-grid-scale modes increases by approximately 15% with each halving of timestep. Scales of low-level rotational motion are larger (near synoptic scales) in the 1800s simulations, indicating that dt_{phys} is subtly modulating the shape of the spectrum.

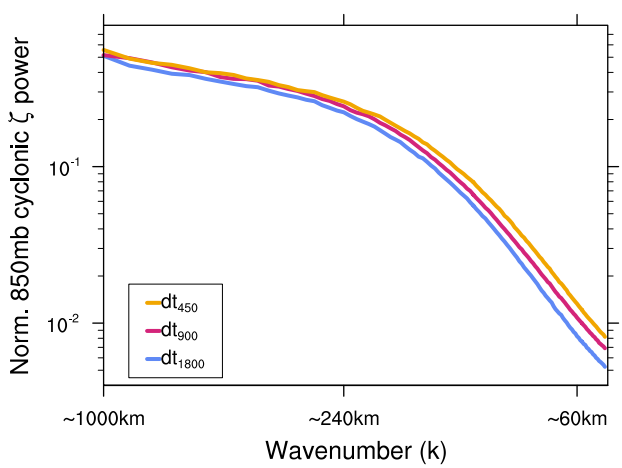

Figure 7. Normalized spectral decomposition for August, September, and October 850 hPa cyclonic relative vorticity (ζ_{850}) as a function of wavenumber. Six-hourly instantaneous values are used. All grid points within 5° of a tracked tropical cyclone are set to zero before computation. Approximate relationship of grid spacing to wavenumber is denoted along the x-axis.

Since existing TCs have been removed, the implication is that the dt_{450} simulations are aggregating near-surface vorticity at scales closer to the resolvable limit of the model when compared to longer timesteps. Since TCs are only well-permitted at grid spacings of approximately 50 km (Walsh et al., 2015; Zhao & Held, 2012), this provides preferential accumulation of rotational motion at scales small enough for spontaneous TC genesis to more frequently occur in the dt_{450} configuration.

Finally, this can be further substantiated by an analysis of discrete TC seeds. Figure 8 shows the genesis density of TC seeds for each of the three configurations. Seeds are tracked using the methodology in Section 2.3 and the first point of a trajectory where the seed criteria are satisfied is defined as genesis. As with TC frequency, there is a monotonic relationship of seeds with dt_{phys}. The ratio of the number of seeds (annotation in Figure 8 insets) to the number of TCs (Table 2) within a basin implies that the probability of a seed becoming a TC (approximately 30%–50% here) is comparatively similar. While it should be noted that the seed definition used here does not require a tracked TC to be tied to a specific seed, the fact that this ratio is closer across the simulations than the absolute TC counts themselves would indicate that the timestep sensitivity arises from shorter timescales modulating the TC precursor environment.

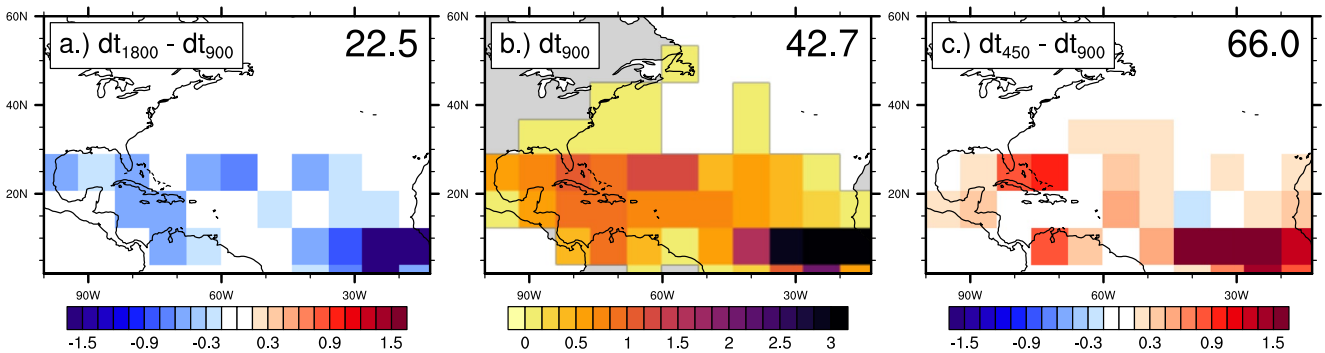

Figure 8. Annual genesis density of tropical cyclone seeds per year for the dt_{900} simulation (center) with difference of the dt_{1800} (dt_{450}) simulations relative to the dt_{900} simulation on the left (right). Units are seed genesis events per 8° × 8° box per year. Basin-wide frequency of seeds per year are denoted in top right of each panel.

Viewing this small-scale variability from either an Eulerian (Figures 5–7) or Lagrangian (Figure 8) perspective offer the same insight: an increase in precursor, sub-TC intensity features in the simulations with shorter dt_{phys} (i.e., increased coupling frequency).

4. Sensitivity Experiments

While we have demonstrated that the simulated TC frequency in CAM5 is sensitive to timestep and have validated that this arises due to differences in the small-scale, short-term variability aspects of the NATL, we seek further confirmation that this is indeed due to shifts in the convective versus large-scale partitioning of precipitation. In order to do so, we perform two sets of sensitivity experiments with the same dt_{phys}. In the first experiment, we apply dt_{phys} of 450s but reduce τ from its hardcoded value of 3600s to 900s. Given Equation 3, a reduction of τ increases the amount of CAPE removed during each call of the convective parameterization, which is called before the large-scale microphysics (Figure 1). Therefore, this serves the purpose of enhancing convective rainfall which tilts the "competition" for column stabilization back toward the deep convective routine, even in the presence of a short dt_{phys} (Williamson, 2013). This run is referred to as $dt_{450,\tau-}$.

In our second experiment, we repeat the dt_{450} experiment where $\tau = 3600$s, except we reduce the deep convective entrainment rate (dmpdz) from the default of 1×10^{-3} to 0.3×10^{-3} m^{-1}. By decreasing the magnitude of this value, the mixing of cool and dry air parcels into convective plumes is reduced. Past work has shown this parameter to be important for the vertical extent of convection (Rasch et al., 2019; Xie et al., 2018), simulated precipitation (Bernstein & Neelin, 2016; Qian et al., 2015) and, in particular, the evolution of TCs (He & Posselt, 2015). Since entrainment is a mechanism that weakens subgrid convection, its reduction means that CAPE (and subsequently CAPE consumption) is enhanced, allowing it to effectively remove more instability before the resolved scale microphysics is subsequently called. This tilts the competition back "toward" the deep convective parameterization, even with a small dt_{phys} and long τ.

It must be emphasized that neither of these necessarily "undo" the impact of timestep sensitivity, but rather, provide alternative mechanisms for adjusting the competition between subgrid parameterizations in the absence of modification to the timescales themselves. If this competition between precipitation mechanisms and their associated forcing scales are indeed the driver in TC frequency changes, we would expect the two sensitivity runs to produce climatological statistics more akin to the dt_{1800} runs due to increased convective activity, even with a shorter timestep.

Table 4 shows the bulk TC statistics (top) and climatological means (bottom) for the two sensitivity runs with dt_{450} also reproduced for reference. Both the $dt_{450,\tau-}$ and $dt_{450,dmpdz}$ simulations result in vastly reduced TC activity, with annual frequency being reduced from 19.5 TCs yr^{-1} to 6.1 and 5.8, respectively. Similar decreases on a proportional basis are seen in TCD and ACE. Seeds also decrease accordingly, although the decrease in these features is larger in $dt_{450,\tau-}$, to the point where the number of seeds (which are restricted to ASO and being equatorward of 30°N) occur with less climatological frequency than basin-wide TCs themselves (which have no such spatiotemporal restrictions). This may imply this particular configuration has altered pathways for TC genesis (e.g., high-latitude or out-of-season TCs) although confirming this is beyond the scope of this paper.

Table 4
As in Tables 2 and 3, Except for the dt_{450}, $dt_{450,dmpdz}$, and $dt_{450,\tau-}$ Simulations

Variable	Units	dt_{450}	$dt_{450,\tau-}$	$dt_{450,dmpdz}$
n	# yr^{-1}	19.5 (5.4)	6.0 (3.2)	5.8 (2.6)
TCD	days yr^{-1}	125.6 (32.6)	36.5 (23.2)	36.8 (23.1)
ACE	kn yr^{-1}	132.2 (60.0)	29.6 (26.1)	36.5 (32.0)
TC "seeds"	# yr^{-1}	66.0 (19.5)	5.8 (3.2)	15.3 (5.4)
Large-scale precipitation rate (PRECL)	mm day^{-1}	1.05	0.34	0.31
Convective precipitation rate (PRECC)	mm day^{-1}	3.09	3.60	3.64
Total precipitation rate (PRECT)	mm day^{-1}	4.14	3.93	3.95
Precipitation ratio (PRECL/PRECC)	–	0.34	0.09	0.09
500 hPa pressure velocity (ω_{500})	Pa s^{-1}	-5.69×10^{-3}	-3.13×10^{-3}	-5.24×10^{-3}
Maximum potential intensity (MPI)	m s^{-1}	72.3	72.3	72.9
Saturation entropy deficit (χ_m)	–	0.51	0.55	0.55
Relative vorticity (ζ)	10^5 s^{-1}	−0.16	−0.15	−0.07
850-250 hPa wind shear (VSHEAR)	m s^{-1}	4.27	4.25	4.14

Note. Tropical cyclones "seeds" have been added to the annual climatology statistics.

When τ is reduced to 900s, the ratio of large-scale to convective precipitation is reduced, as expected. The same response is seen when decreasing dmpdz, confirming the "reactivation" of the deep convective parameterization, even with a longer τ. As before, large-scale climatological ASO averages over the North Atlantic basin are relatively unchanged in the three runs. In particular, MPI, χ_m, and vertical wind shear are within a few percent of one another. Larger changes are noted in vertical motion (relative vorticity) for the $dt_{450,\tau-}$ ($dt_{450,dmpdz}$) runs, indicating the potential for more systematic changes in the mean state with fundamental modifications to the parameterizations (vs. just changing the timestep). In particular, the activity of ZM as measured by tendencies of deep convective temperature and moisture over the North Atlantic is significantly increased in the $dt_{450,dmpdz}$ simulations (moreso than $dt_{450,\tau-}$, not shown). While these merit further exploration in the future, the runs have modified the PRECC/PRECL ratio in the desired manner, therefore we continue to focus on the distribution of extreme values of vertical velocity and precipitation as above.

Figure 9 shows the same results as in Figure 5, except for the sensitivity runs (dt_{450} is reproduced in orange). Interestingly, the convective precipitation frequency changes more for $dt_{450,\tau-}$ than $dt_{450,dmpdz}$ (Figure 9a). The exact reason for this is not clear, although $dt_{450,dmpdz}$ has a higher frequency of weaker rates, perhaps implying that ZM is being triggered more often in that run. The ZM temperature and moisture tendencies occur over a slightly deeper portion of the atmosphere in $dt_{450,dmpdz}$ (not shown, but also as noted in the previous studies referenced above),

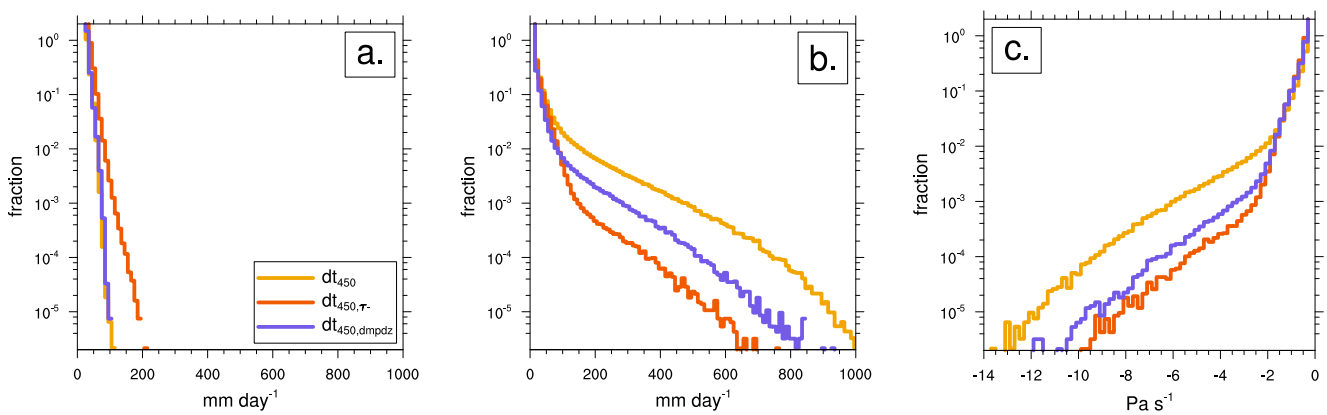

Figure 9. As in Figure 5 except for the dt_{450} (orange), $dt_{450,\tau-}$ (red), and $dt_{450,dmpdz}$ (purple) simulations.

which also may be playing a role. However, most relevant here is that decreased τ and increased dmpdz both serve to reduce extremes in the tail of the large-scale precipitation and vertical velocity distributions (Figures 9b and 9c), expected given the reduction in resolved-scale precipitation shown in Table 4 and akin to the sensitivity to physics timestep.

Additional confirmation of this is shown in Figure 10, which shows reduced power in cyclonic vorticity at smaller spatial scales in the sensitivity runs. Reducing τ while holding dt_{phys} fixed results in a response analogous to increasing dt_{phys} while holding τ fixed (Figure 7). Further, we see that even with a high τ to dt_{phys} ratio, the modified entrainment experiment produces a spectrum that implies reduced TC genesis relative to dt_{450}.

These results show that the TC frequency in the model is indeed highly sensitive to the tradeoff between the deep convective and large-scale parameterizations. The same sensitivity to dt_{phys} when going from 1800 to 450s can be reproduced via a targeted experiment designed to offset the reduced convective activity in dt_{450} with artificial enhancement via parameter modifications to the ZM scheme.

5. Discussion

5.1. Summary of Findings

In this manuscript we demonstrate that the number of TCs simulated in a free-running high-resolution GCM can be sensitive to the physics timestep. Keeping all aspects of the model configuration identical while only changing the timestep from 1800 to 450s results in an increase of greater than 80% in annual simulated TCs over the North Atlantic basin even though the mean summer large-scale climatology is far less sensitive to these changes.

A potential interpretation is diagrammed in Figure 11. Shorter dt_{phys} results in less CAPE removal by the deep convective parameterization and therefore more intense grid-scale precipitation rates, which correspondingly drive more intense vertical velocities. This larger vertical mass flux drives enhanced low-level convergence (and stronger surface enthalpy fluxes), which accumulate low-level vorticity near the grid-scale. Spatially compact regions of cyclonic vorticity serve as "seeds" for simulated TCs. Since the environmental large-scale conditions that precede storm genesis are highly similar between the configurations, the probability of a seed becoming a TC is relatively similar. Therefore, it is the increase in these "seeds" that lead to the higher TC frequency associated with shorter dt_{phys}.

It is known that models with CAPE-dependent deep convective parameterizations which become "less active" will simulate enhanced resolved (i.e., near the grid scale) moist convective motions (McTaggart-Cowan et al., 2020). The particular behavior outlined here is a fundamental response to the timescales over which moist processes are operating within the model. A possible explanation for this response is laid out in Williamson (2013). Two processes engage in competition to remove atmospheric instabilities. The total CAPE consumed by the deep convective parameterization over a physics timestep will be equal to $F \times M_b \times dt_{phys}$. In the current configuration of ZM in CAM, τ is a fixed parameter. Given that τ is fixed, for a given convectively unstable column, the ability of the convective parameterization to remove instability over a single timestep will scale directly with the length of that timestep. Therefore, in a sequential update formulation, such as in the CAM physics, a shorter dt_{phys} requires additional resolved scale overturning in order to remove column convective instability. This leads to more (less) local grid-scale (diffuse) latent heating, subsequent resolved vertical motions, enhancement of surface enthalpy fluxes, and small-scale aggregation of surface convergence in the presence of sufficient planetary vorticity to generate TCs.

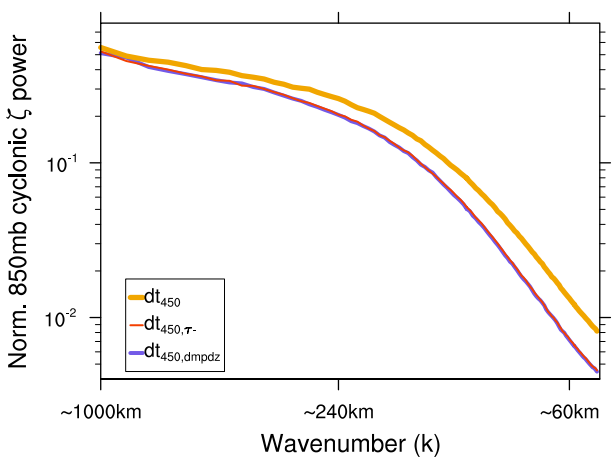

Figure 10. As in Figure 7 except for the dt_{450}, $dt_{450,dmpdz}$, and $dt_{450,\tau-}$ simulations. Note that the $dt_{450,\tau-}$ curve partially overlays the $dt_{450,dmpdz}$ one.

From a process standpoint, this response is also highly similar to that observed by Zhao et al. (2012) when modifying the entrainment within the convective parameterization. However, it is critical to note that the behavior described here is not fundamentally a parameterization design choice but can occur across multiple simulations using identical code bases and tuning

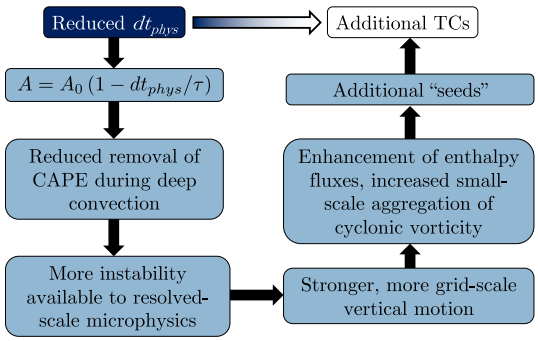

Figure 11. Schematic of mechanism that leads to the relationship between dt_{phys} and the annual frequency of simulated tropical cyclones in the Community Atmosphere Model.

configurations. Both Reed et al. (2012) and X. Li et al. (2020) also found a sensitivity to timestep in TC simulations and noted changes in moist process partitioning, although it is important to note that their analyses were conditional on the a priori existence of a TC, whereas this research explicitly focuses on the spontaneous genesis of such storms in free-running simulations. Somewhat interestingly, timestep sensitivity to the intensity of mature TCs in the simulations here is relatively small, likely owing to the fact that the inner core processes of TCs in CAM5 are dominated by resolved-scale processes.

While the sensitivity experiments in Section 4 clearly show that the relationship between dt_{phys} and τ contributes to a change in TCs, all else equal, additional feedbacks associated with the convective-resolved scale partitioning that go beyond strictly changes in ZM CAPE consumption are likely playing a role. Herrington and Reed (2018) found changes in vertical velocity distributions when changing the physics timestep, even in the absence of a convective parameterization, hypothesizing that this behavior arises due to time truncation errors when the ratio of dt_{phys} to dt_{dyn} becomes large. Here, a brief set of runs with the deep convective parameterization turned off and dt_{phys} varied between 450 and 1800s was also completed. While the sensitivity was reduced relative to that outlined above, TCs also decreased with increasing dt_{phys}, although these simulations also suffered from numerical instabilities (not shown). While a deeper investigation of this requires additional model runs and is beyond the scope of this paper, all of the above implies that multiple errors that amplify or offset one another likely exist and that gaps in published PDC literature remain in need of addressing. More idealized (e.g., Herrington and Reed (2020)) or convective-permitting experiments (e.g., Stevens et al. (2019)) may provide pathways for better understanding these responses.

Models with O(25 km) resolution are considered "high-resolution" in the climate community and will likely be used for global weather impacts research for at least the next decade, if not longer. In many cases, GCMs are designed and tuned to work at coarser resolutions and longer timesteps. Higher-resolution simulations require shorter dt_{phys} for both stability and to ensure resolved flow does not "drift" too far from the subgrid physics between couplings. However, the added cost associated with tighter coupling is not insignificant (e.g., Table 2). Relatedly, while a formal convergence study at even smaller dt_{phys} was not computationally feasible here, it is worth noting that Wan et al. (2015) found considerably weaker than expected solution convergence with CAM5-SE, even down to dt_{phys} of 1s. Their findings underscore that the solutions to challenges such as those noted here are not necessarily solved by blindly increasing computational expense.

One important consideration is the use of numerical models for understanding controls on TC frequency and how TC frequency will change in the future. It is clear that O(25 km) simulations permit TCs, although they under-resolve small-scale storm features (Davis, 2018). This likely puts models in a resolution space where the resolved scale dynamics cannot wholly support a realistic observed TC climatology, but parameterized moist processes can provide thermodynamic support to sustain more reasonable statistics. Living at this resolved/unresolved interface requires extreme care in simulation design, however, as convective gray zone modelers (Gao et al., 2017) can certainly attest.

It is also unclear how these choices upscale back into the global climate system. For example, Zarzycki and Jablonowski (2014) noted higher values of transient meridional momentum flux over the NATL during summer months in simulations with more TCs. Making the (highly) idealistic argument that time step only impacts TC frequency, this "bridge" could serve as a mechanism to impact other teleconnected aspects of the climate system.

5.2. Moving Forward

The question then becomes, how should this be addressed? The most physically consistent pathway may be to minimize substepping and more tightly couple the physics and dynamics in time, as is generally done in numerical weather prediction models (e.g., Skamarock and Klemp (2008)). This may also serve to address potential time truncation errors, such as those hypothesized by Herrington and Reed (2018). However, this may remain compu-

tationally challenging for global models that need to be integrated for weeks to centuries (Gross et al., 2018). Improved emphasis on optimized and scalable source code (e.g., Dennis et al. (2012)) may benefit this endeavor.

One possibility is to tie τ to dt_{phys} such that timescales are adjusted in a consistent fashion. This method was explored by Williamson (2013) and has been utilized in a few resolution-sensitivity studies over the past few years. In general, taking care to adjust timescales in a consistent manner across parameterizations produces results that are less sensitive to timestep, although substantial non-linearities in subgrid physics packages make it effectively impossible to guarantee strict convergence. In fact, in this study changing dt_{phys} while keeping the ratio of dt_{phys} and τ constant still resulted in differing climatologies (see dt_{1800} and $dt_{450,\tau-}$).

Another option is to scale τ with horizontal resolution rather than timestep to attempt to better balance the tradeoff between convective and large-scale precipitation at different resolutions. This has not been done in TC simulations, but has been tried elsewhere (Gustafson et al., 2014; Ma et al., 2014). An analogous version of this method was proposed by Arakawa and Wu (2013) as a mechanism for scale-aware physics. One could also modify τ in a profile- or flow-dependent manner, although there are no obvious examples in literature. It is worth noting that tying the timescale to resolution or flow does not explicitly account for the timestep sensitivity here, but may offer implicit solutions by modifying the parameterized versus resolved precipitation ratios.

A final wrinkle is defining the role of convective parameterization itself in high-resolution simulations. Rauscher et al. (2016) and Herrington and Reed (2020) both quantify how vertical velocities become more intense as grid spacing decreases. In practice, this more intense resolved scale motion explains why large-scale precipitation increases as resolution increases - effectively, the resolved scales are augmenting convective parameterizations in convective regimes. However, Williamson (2008) and O'Brien et al. (2013) beg the question: if one considers convective precipitation truly the subgrid representation of convection, then should convective precipitation rates change as a function of resolution in regimes unable to permit convection? Viewing through this lens (rather than the simple "tradeoff" used in this manuscript) requires higher-order consideration of not only total, mean precipitation, but also changes in rate and frequency as a function of resolution, adding another layer of complexity. Since we are only focused on the timestep sensitivity at a constant grid spacing, resolution sensitivity is not directly applicable here, although it is obvious to see the entanglement of the two.

While all of these methods serve to mitigate timestep sensitivity by providing a more active convective parameterization at higher spatial resolutions, it should be noted that models at high resolution with vigorous convective parameterization tend to suffer from poorly simulated diurnal cycles of precipitation. Therefore, one could imagine a reduced τ improving TC climatology but negatively impacting precipitation timing over land surfaces, underscoring the difficulties in tuning moist parameterizations. More involved solutions may involve replacing parameterizations with either unified approaches (e.g., Golaz et al. (2002)) or scale-aware methods (e.g., Grell and Freitas (2014)).

There is no "silver bullet," since GCMs are rarely tuned to target a specific phenomenon. Rather, the aim of this paper is to highlight this sensitivity; extreme caution should be undertaken when evaluating model solutions that target phenomena that rely on both resolved-scale and parameterized moist processes. Generalizing about TC-climate theory using high-resolution GCMs should ensure that results are robust to multiple timesteps and coupling strategies. Stakeholders and other end users of climate data should also be aware of such behaviors and make decisions on the credibility of existing datasets on a case-by-case basis.

Data Availability Statement

The Community Earth System Model (CESM, Danabasoglu et al. (2020)) tag used in these simulations is "cesm2_0_beta08" and can be downloaded from the CESM code repository at https://github.com/ESCOMP/CESM. IBTrACS v4 (Knapp et al., 2010) was downloaded from the NOAA National Centers for Environmental Information at https://doi.org/10.25921/82ty-9e16. TempestExtremes (Ullrich & Zarzycki, 2017; Ullrich et al., 2021) was used to track both TCs and seeds and can be downloaded from https://github.com/ClimateGlobalChange/tempestextremes. Storm statistics and spatial plots were generated using the Cyclone Metrics Package (CyMeP, Zarzycki et al. (2021)) which can be downloaded from https://github.com/zarzycki/cymep. All data used to generate the figures contained in this manuscript are archived via Zenodo at doi:10.5281/zenodo.6334837.

Acknowledgments
The author acknowledges three anonymous reviewers, whose feedback greatly improved this manuscript. This material is based upon work supported as part of a Climate Process Team (CPT) under Grant AGS-1916689 from the National Science Foundation and Grant NA19OAR4310363 from the National Oceanic and Atmospheric Administration. The author acknowledges high-performance computing support from Cheyenne (https://doi:10.5065/D6RX99HX) provided by NCAR's Computational and Information Systems Laboratory, sponsored by the National Science Foundation. The author thanks Adam Herrington, who provided useful thoughts on an early draft of this manuscript.

References

Arakawa, A. (2004). The cumulus parameterization problem: Past, present, and future. *Journal of Climate*, *17*(13), 2493–2525. https://doi.org/10.1175/1520-0442(2004)017<2493:ratcpp>2.0.co;2

Arakawa, A., & Wu, C.-M. (2013). A unified representation of deep moist convection in numerical modeling of the atmosphere. Part I. *Journal of the Atmospheric Sciences*, *70*(7), 1977–1992. https://doi.org/10.1175/JAS-D-12-0330.1

Bacmeister, J. T., Wehner, M. F., Neale, R. B., Gettelman, A., Hannay, C., Lauritzen, P. H., & Truesdale, J. E. (2014). Exploratory high-resolution climate simulations using the Community Atmosphere Model (CAM). *Journal of Climate*, *27*(9), 3073–3099. https://doi.org/10.1175/JCLI-D-13-00387.1

Barrett, A. I., Wellmann, C., Seifert, A., Hoose, C., Vogel, B., & Kunz, M. (2019). One step at a time: How model time step significantly affects convection-permitting simulations. *Journal of Advances in Modeling Earth Systems*, *11*(3), 641–658. https://doi.org/10.1029/2018MS001418

Beljaars, A., Balsamo, G., Bechtold, P., Bozzo, A., Forbes, R., Hogan, R. J., & Wedi, N. (2018). The numerics of physical parametrization in the ECMWF model. *Frontiers in Earth Science*, *6*, 137. https://doi.org/10.3389/feart.2018.00137

Beljaars, A., Bechtold, P., Köhler, M., Morcrette, J.-J., Tompkins, A., Viterbo, P., & Wedi, N. (2004). The numerics of physical parameterization. In *Seminar on recent developments in numerical methods for atmospheric and ocean modelling, 6–10 september 2004* (pp. 113–134). ECMWF.

Bell, G. D., Halpert, M. S., Schnell, R. C., Higgins, R. W., Lawrimore, J., Kousky, V. E., & Artusa, A. (2000). Climate assessment for 1999. *Bulletin of the American Meteorological Society*, *81*(6), S1–S50. https://doi.org/10.1175/1520-0477(2000)81[s1:caf]2.0.co;2

Bernstein, D. N., & Neelin, J. D. (2016). Identifying sensitive ranges in global warming precipitation change dependence on convective parameters. *Geophysical Research Letters*, *43*(11), 5841–5850. https://doi.org/10.1002/2016GL069022

Bister, M., & Emanuel, K. A. (2002). Low frequency variability of tropical cyclone potential intensity 1. Interannual to interdecadal variability. *Journal of Geophysical Research*, *107*(D24). https://doi.org/10.1029/2001JD000776

Bruyère, C. L., Holland, G. J., & Towler, E. (2012). Investigating the use of a genesis potential index for tropical cyclones in the North Atlantic Basin. *Journal of Climate*, *25*(24), 8611–8626. https://doi.org/10.1175/JCLI-D-11-00619.1

Camargo, S. J., Emanuel, K. A., & Sobel, A. H. (2007). Use of a genesis potential index to diagnose ENSO effects on tropical cyclone genesis. *Journal of Climate*, *20*(19), 4819–4834. https://doi.org/10.1175/JCLI4282.1

Camargo, S. J., Giulivi, C. F., Sobel, A. H., Wing, A. A., Kim, D., Moon, Y., et al. (2020). Characteristics of model tropical cyclone climatology and the large-scale environment. *Journal of Climate*, *33*(11), 4463–4487. https://doi.org/10.1175/JCLI-D-19-0500.1

Danabasoglu, G., Lamarque, J.-F., Bacmeister, J., Bailey, D., DuVivier, A., Edwards, J., et al. (2020). The Community Earth System Model version 2 (CESM2). *Journal of Advances in Modeling Earth Systems*, *12*(2). https://doi.org/10.1029/2019ms001916

Davis, C. (2018). Resolving tropical cyclone intensity in models. *Geophysical Research Letters*, *45*(4), 2082–2087. https://doi.org/10.1002/2017GL076966

DeMaria, M., Knaff, J. A., & Connell, B. H. (2001). A tropical cyclone genesis parameter for the tropical Atlantic. *Weather and Forecasting*, *16*(2), 219–233. https://doi.org/10.1175/1520-0434(2001)016<0219:atcgpf>2.0.co;2

Dennis, J. M., Edwards, J., Evans, K. J., Guba, O., Lauritzen, P. H., Mirin, A. A., & Worley, P. H. (2012). CAM-SE: A scalable spectral element dynamical core for the Community Atmosphere Model. *International Journal of High Performance Computing Applications*, *26*(1), 74–89. https://doi.org/10.1177/1094342011428142

Donahue, A. S., & Caldwell, P. M. (2018). Impact of physics parameterization ordering in a global atmosphere model. *Journal of Advances in Modeling Earth Systems*, *10*(2), 481–499. https://doi.org/10.1002/2017MS001067

Donahue, A. S., & Caldwell, P. M. (2020). Performance and accuracy implications of parallel split physics-dynamics coupling in the Energy Exascale Earth System Atmosphere Model. *Journal of Advances in Modeling Earth Systems*, *12*(7), e2020MS002080. https://doi.org/10.1029/2020MS002080

Emanuel, K. (2010). Tropical cyclone activity downscaled from NOAA-CIRES reanalysis, 1908–1958. *Journal of Advances in Modeling Earth Systems*, *2*(1). https://doi.org/10.3894/JAMES.2010.2.1

Emanuel, K. (2013). Downscaling CMIP5 climate models shows increased tropical cyclone activity over the 21st century. *Proceedings of the National Academy of Sciences*, *110*(30), 12219–12224. https://doi.org/10.1073/pnas.1301293110

Errico, R. M. (1985). Spectra computed from a limited area grid. *Monthly Weather Review*, *113*(9), 1554–1562. https://doi.org/10.1175/1520-0493(1985)113<1554:scfala>2.0.co;2

Frank, W. M. (1983). The cumulus parameterization problem. *Monthly Weather Review*, *111*(9), 1859–1871. https://doi.org/10.1175/1520-0493(1983)111<1859:tcpp>2.0.co;2

Gao, Y., Leung, L. R., Zhao, C., & Hagos, S. (2017). Sensitivity of US summer precipitation to model resolution and convective parameterizations across gray zone resolutions. *Journal of Geophysical Research: Atmospheres*, *122*(5), 2714–2733. https://doi.org/10.1002/2016JD025896

Garratt, J. R. (1992). *The atmospheric boundary layer*. Cambridge University Press. 316.

Gates, W. L., Boyle, J. S., Covey, C. C., Dease, C. G., Doutriaux, C. M., Drach, R. S., & Williams, D. N. (1999). An overview of the results of the atmospheric model intercomparison project (AMIP I). *Bulletin of the American Meteorological Society*, *80*, 29–55. https://doi.org/10.1175/1520-0477(1999)080<0029:aootro>2.0.co;2

Gettelman, A., Liu, X., Ghan, S. J., Morrison, H., Park, S., Conley, A. J., & Li, J.-L. F. (2010). Global simulations of ice nucleation and ice supersaturation with an improved cloud scheme in the Community Atmosphere Model. *Journal of Geophysical Research: Atmospheres*, *115*(D18). https://doi.org/10.1029/2009JD013797

Gettelman, A., & Morrison, H. (2015). Advanced two-moment bulk microphysics for global models. Part I: Off-line tests and comparison with other schemes. *Journal of Climate*, *28*(3), 1268–1287. https://doi.org/10.1175/JCLI-D-14-00102.1

Golaz, J.-C., Larson, V. E., & Cotton, W. R. (2002). A PDF-based model for boundary layer clouds. Part I: Method and model description. *Journal of the Atmospheric Sciences*, *59*(24), 3540–3551. https://doi.org/10.1175/1520-0469(2002)059<3540:apbmfb>2.0.co;2

Goldenberg, S. B., & Shapiro, L. J. (1996). Physical mechanisms for the association of El Niño and West African rainfall with Atlantic major hurricane activity. *Journal of Climate*, *9*(6), 1169–1187. https://doi.org/10.1175/1520-0442(1996)009<1169:pmftao>2.0.co;2

Grell, G. A., & Freitas, S. R. (2014). A scale and aerosol aware stochastic convective parameterization for weather and air quality modeling. *Atmospheric Chemistry and Physics*, *14*(10), 5233–5250. https://doi.org/10.5194/acp-14-5233-2014

Gross, M., Wan, H., Rasch, P. J., Caldwell, P. M., Williamson, D. L., Klocke, D., & Leung, R. (2018). Physics-dynamics coupling in weather, climate, and Earth system models: Challenges and recent progress. *Monthly Weather Review*, *146*(11), 3505–3544. https://doi.org/10.1175/MWR-D-17-0345.1

Guimond, S. R., Reisner, J. M., Marras, S., & Giraldo, F. X. (2016). The impacts of dry dynamic cores on asymmetric hurricane intensification. *Journal of the Atmospheric Sciences*, *73*(12), 4661–4684. https://doi.org/10.1175/JAS-D-16-0055.1

Gustafson, W. I., Jr, Ma, P.-L., & Singh, B. (2014). Precipitation characteristics of CAM5 physics at mesoscale resolution during MC3E and the impact of convective timescale choice. *Journal of Advances in Modeling Earth Systems*, *6*(4), 1271–1287. https://doi.org/10.1002/2014MS000334

He, F., & Posselt, D. J. (2015). Impact of parameterized physical processes on simulated tropical cyclone characteristics in the Community Atmosphere Model. *Journal of Climate*, *28*(24), 9857–9872. https://doi.org/10.1175/JCLI-D-15-0255.1

Herrington, A. R., & Reed, K. A. (2018). An idealized test of the response of the Community Atmosphere Model to near-grid-scale forcing across hydrostatic resolutions. *Journal of Advances in Modeling Earth Systems*, *10*(2), 560–575. https://doi.org/10.1002/2017MS001078

Herrington, A. R., & Reed, K. A. (2020). On resolution sensitivity in the Community Atmosphere Model. *Quarterly Journal of the Royal Meteorological Society*, *146*(733), 3789–3807. https://doi.org/10.1002/qj.3873

Hourdin, F., Mauritsen, T., Gettelman, A., Golaz, J.-C., Balaji, V., Duan, Q., & Williamson, D. (2017). The art and science of climate model tuning. *Bulletin of the American Meteorological Society*, *98*(3), 589–602. https://doi.org/10.1175/BAMS-D-15-00135.1

Hsieh, T.-L., Vecchi, G. A., Yang, W., Held, I. M., & Garner, S. T. (2020). Large-scale control on the frequency of tropical cyclones and seeds: A consistent relationship across a hierarchy of global atmospheric models. *Climate Dynamics*, *55*(11), 3177–3196. https://doi.org/10.1007/s00382-020-05446-5

Hurrell, J. W., Hack, J. J., Shea, D., Caron, J. M., & Rosinski, J. (2008). A new sea surface temperature and sea ice boundary dataset for the Community Atmosphere Model. *Journal of Climate*, *21*(19), 5145–5153. https://doi.org/10.1175/2008JCLI2292.1

Hurrell, J. W., Holland, M. M., Gent, P. R., Ghan, S., Kay, J. E., Kushner, P. J., & Marshall, S. (2013). The Community Earth System Model: A framework for collaborative research. *Bulletin of the American Meteorological Society*, *94*(9), 1339–1360. https://doi.org/10.1175/BAMS-D-12-00121.1

Kim, D., Sobel, A. H., Del Genio, A. D., Chen, Y., Camargo, S. J., Yao, M.-S., & Nazarenko, L. (2012). The tropical subseasonal variability simulated in the NASA GISS general circulation model. *Journal of Climate*, *25*(13), 4641–4659. https://doi.org/10.1175/JCLI-D-11-00447.1

Knapp, K. R., Kruk, M. C., Levinson, D. H., Diamond, H. J., & Neumann, C. J. (2010). The International Best Track Archive for Climate Stewardship (IBTrACS). *Bulletin of the American Meteorological Society*, *91*(3), 363–376. https://doi.org/10.1175/2009BAMS2755.1

Lauritzen, P. H., Nair, R. D., Herrington, A. R., Callaghan, P., Goldhaber, S., Dennis, J. M., & Tribbia, J. J. (2018). NCAR release of CAM-SE in CESM2.0: A reformulation of the spectral element dynamical core in dry-mass vertical coordinates with comprehensive treatment of condensates and energy. *Journal of Advances in Modeling Earth Systems*, *10*(7), 1537–1570. https://doi.org/10.1029/2017MS001257

Lawrence, D. M., Fisher, R. A., Koven, C. D., Oleson, K. W., Swenson, S. C., Bonan, G., & Zeng, X. (2019). The Community Land Model version 5: Description of new features, benchmarking, and impact of forcing uncertainty. *Journal of Advances in Modeling Earth Systems*, *11*(12), 4245–4287. https://doi.org/10.1029/2018MS001583

Li, H., & Sriver, R. L. (2018). Tropical cyclone activity in the high-resolution Community Earth System Model and the impact of ocean coupling. *Journal of Advances in Modeling Earth Systems*, *10*(1), 165–186. https://doi.org/10.1002/2017MS001199

Li, X., Peng, X., & Zhang, Y. (2020). Investigation of the effect of the time step on the physics-dynamics interaction in CAM5 using an idealized tropical cyclone experiment. *Climate Dynamics*, *55*(3), 665–680. https://doi.org/10.1007/s00382-020-05284-5

Lim, Y.-K., Schubert, S. D., Reale, O., Lee, M.-I., Molod, A. M., & Suarez, M. J. (2015). Sensitivity of tropical cyclones to parameterized convection in the NASA GEOS-5 model. *Journal of Climate*, *28*(2), 551–573. https://doi.org/10.1175/JCLI-D-14-00104.1

Ma, P.-L., Rasch, P. J., Fast, J. D., Easter, R. C., Gustafson, W. I., Jr, Liu, X., & Singh, B. (2014). Assessing the CAM5 physics suite in the WRF-chem model: Implementation, resolution sensitivity, and a first evaluation for a regional case study. *Geoscientific Model Development*, *7*(3), 755–778. https://doi.org/10.5194/gmd-7-755-2014

McTaggart-Cowan, R., Vaillancourt, P. A., Separovic, L., Corvec, S., & Zadra, A. (2020). A convection parameterization for low-CAPE environments. *Monthly Weather Review*, *148*(12), 4917–4941. https://doi.org/10.1175/MWR-D-20-0020.1

Mendelsohn, R., Emanuel, K., Chonabayashi, S., & Bakkensen, L. (2012). The impact of climate change on global tropical cyclone damage. *Nature Climate Change*, *2*(3), 205–209. https://doi.org/10.1038/nclimate1357

Mishra, S. K., & Sahany, S. (2011). Effects of time step size on the simulation of tropical climate in NCAR-CAM3. *Climate Dynamics*, *37*(3), 689–704. https://doi.org/10.1007/s00382-011-0994-4

Morrison, H., & Gettelman, A. (2008). A new two-moment bulk stratiform cloud microphysics scheme in the Community Atmosphere Model, version 3 (CAM3). Part I: Description and numerical tests. *Journal of Climate*, *21*(15), 3642–3659. https://doi.org/10.1175/2008JCLI2105.1

Neale, R. B., Chen, C.-C., Gettelman, A., Lauritzen, P. H., Park, S., Williamson, D. L., & Taylor, M. A. (2012). *Description of the NCAR Community Atmosphere Model (CAM 5.0) (NCAR technical note nos. NCAR/TN-486+STR)*. National Center for Atmospheric Research.

O'Brien, T. A., Li, F., Collins, W. D., Rauscher, S. A., Ringler, T. D., Taylor, M., & Leung, L. R. (2013). Observed scaling in clouds and precipitation and scale incognizance in regional to global atmospheric models. *Journal of Climate*, *26*(23), 9313–9333. https://doi.org/10.1175/JCLI-D-13-00005.1

Park, S., & Bretherton, C. S. (2009). The University of Washington shallow convection and moist turbulence schemes and their impact on climate simulations with the Community Atmosphere Model. *Journal of Climate*, *22*(12), 3449–3469. https://doi.org/10.1175/2008JCLI2557.1

Park, S., Bretherton, C. S., & Rasch, P. J. (2014). Integrating cloud processes in the Community Atmosphere Model, version 5. *Journal of Climate*, *27*(18), 6821–6856. https://doi.org/10.1175/JCLI-D-14-00087.1

Peng, M. S., Fu, B., Li, T., & Stevens, D. E. (2012). Developing versus nondeveloping disturbances for tropical cyclone formation. Part I: North Atlantic. *Monthly Weather Review*, *140*(4), 1047–1066. https://doi.org/10.1175/2011MWR3617.1

Qian, Y., Yan, H., Hou, Z., Johannesson, G., Klein, S., Lucas, D., & Zhao, C. (2015). Parametric sensitivity analysis of precipitation at global and local scales in the Community Atmosphere Model CAM5. *Journal of Advances in Modeling Earth Systems*, *7*(2), 382–411. https://doi.org/10.1002/2014MS000354

Rasch, P. J., Xie, S., Ma, P.-L., Lin, W., Wang, H., Tang, Q., & Yang, Y. (2019). An overview of the atmospheric component of the Energy Exascale Earth System Model. *Journal of Advances in Modeling Earth Systems*, *11*(8), 2377–2411. https://doi.org/10.1029/2019MS001629

Rauscher, S. A., O'Brien, T. A., Piani, C., Coppola, E., Giorgi, F., Collins, W. D., & Lawston, P. M. (2016). A multimodel intercomparison of resolution effects on precipitation: Simulations and theory. *Climate Dynamics*, *47*(7), 2205–2218. https://doi.org/10.1007/s00382-015-2959-5

Reed, K. A., Bacmeister, J. T., Rosenbloom, N. A., Wehner, M. F., Bates, S. C., Lauritzen, P. H., & Hannay, C. (2015). Impact of the dynamical core on the direct simulation of tropical cyclones in a high-resolution global model. *Geophysical Research Letters*, *42*(9), 3603–3608. https://doi.org/10.1002/2015GL063974

Reed, K. A., & Jablonowski, C. (2011). Impact of physical parameterizations on idealized tropical cyclones in the Community Atmosphere Model. *Geophysical Research Letters*, *38*(4). https://doi.org/10.1029/2010GL046297

Reed, K. A., Jablonowski, C., & Taylor, M. A. (2012). Tropical cyclones in the spectral element configuration of the Community Atmosphere Model. *Atmospheric Science Letters*, *13*(4), 303–310. https://doi.org/10.1002/asl.399

Reed, K. A., Stansfield, A. M., Wehner, M. F., & Zarzycki, C. M. (2020). Forecasted attribution of the human influence on Hurricane Florence. *Science Advances*, *6*(1). https://doi.org/10.1126/sciadv.aaw9253

Roberts, M. J., Camp, J., Seddon, J., Vidale, P. L., Hodges, K., Vanniere, B., et al. (2020). Impact of model resolution on tropical cyclone simulation using the HighResMIP-PRIMAVERA multimodel ensemble. *Journal of Climate*, *33*(7), 2557–2583. https://doi.org/10.1175/JCLI-D-19-0639.1

Santos, S. P., Caldwell, P. M., & Bretherton, C. S. (2021). Cloud process coupling and time integration in the E3SM Atmosphere Model. *Journal of Advances in Modeling Earth Systems*, *13*(5), e2020MS002359. https://doi.org/10.1029/2020MS002359

Scoccimarro, E., Fogli, P. G., Reed, K. A., Gualdi, S., Masina, S., & Navarra, A. (2017). Tropical cyclone interaction with the ocean: The role of high-frequency (subdaily) coupled processes. *Journal of Climate*, *30*(1), 145–162. https://doi.org/10.1175/JCLI-D-16-0292.1

Skamarock, W. C. (2004). Evaluating mesoscale NWP models using kinetic energy spectra. *Monthly Weather Review*, *132*(12), 3019–3032. https://doi.org/10.1175/MWR2830.1

Skamarock, W. C., & Klemp, J. B. (2008). A time-split nonhydrostatic atmospheric model for weather research and forecasting applications. *Journal of Computational Physics*, *227*(7), 3465–3485. https://doi.org/10.1016/j.jcp.2007.01.037

Smagorinsky, J. (1974). Global atmospheric modeling and numerical simulation of climate. In W. Hess (Ed.), *Weather and climate modification* (pp. 633–686). Wiley and Sons.

Stansfield, A. M., Reed, K. A., & Zarzycki, C. M. (2020). Changes in precipitation from North Atlantic tropical cyclones under RCP scenarios in the variable-resolution Community Atmosphere Model. *Geophysical Research Letters*, *47*(12), e2019GL086930. https://doi.org/10.1029/2019GL086930

Stansfield, A. M., Reed, K. A., Zarzycki, C. M., Ullrich, P. A., & Chavas, D. R. (2020). Assessing tropical cyclones contribution to precipitation over the eastern United States and sensitivity to the variable-resolution domain extent. *Journal of Hydrometeorology*, *21*(7), 1425–1445. https://doi.org/10.1175/JHM-D-19-0240.1

Stevens, B., Satoh, M., Auger, L., Biercamp, J., Bretherton, C. S., Chen, X., & Zhou, L. (2019). DYAMOND: The Dynamics of the atmospheric general circulation modeled on non-hydrostatic domains. *Progress in Earth and Planetary Science*, *6*(1), 1–17. https://doi.org/10.1186/s40645-019-0304-z

Tang, B., & Emanuel, K. (2012). A ventilation index for tropical cyclones. *Bulletin of the American Meteorological Society*, *93*(12), 1901–1912. https://doi.org/10.1175/BAMS-D-11-00165.1

Taylor, M. A., Edwards, J., Thomas, S., & Nair, R. D. (2007). A mass and energy conserving spectral element atmospheric dynamical core on the cubed-sphere grid. *Journal of Physics: Conference Series*, *78*, 012074. https://doi.org/10.1088/1742-6596/78/1/012074

Teixeira, J., Reynolds, C. A., & Judd, K. (2007). Time step sensitivity of nonlinear atmospheric models: Numerical convergence, truncation error growth, and ensemble design. *Journal of the Atmospheric Sciences*, *64*(1), 175–189. https://doi.org/10.1175/JAS3824.1

Thatcher, D. R., & Jablonowski, C. (2016). A moist aquaplanet variant of the Held-Suarez test for atmospheric model dynamical cores. *Geoscientific Model Development*, *9*(4), 1263–1292. https://doi.org/10.5194/gmd-9-1263-2016

Ullrich, P. A., & Zarzycki, C. M. (2017). TempestExtremes: A framework for scale-insensitive pointwise feature tracking on unstructured grids. *Geoscientific Model Development*, *10*(3), 1069–1090. https://doi.org/10.5194/gmd-10-1069-2017

Ullrich, P. A., Zarzycki, C. M., McClenny, E. E., Pinheiro, M. C., Stansfield, A. M., & Reed, K. A. (2021). Tempestextremes v2.1: A community framework for feature detection, tracking, and analysis in large datasets. *Geoscientific Model Development*, *14*(8), 5023–5048. https://doi.org/10.5194/gmd-14-5023-2021

Vitart, F., Anderson, J. L., Sirutis, J., & Tuleya, R. E. (2001). Sensitivity of tropical storms simulated by a general circulation model to changes in cumulus parametrization. *Quarterly Journal of the Royal Meteorological Society*, *127*(571), 25–51. https://doi.org/10.1002/qj.49712757103

Waite, M. L. (2016). Dependence of model energy spectra on vertical resolution. *Monthly Weather Review*, *144*(4), 1407–1421. https://doi.org/10.1175/MWR-D-15-0316.1

Walsh, K. J. E., Camargo, S. J., Vecchi, G. A., Daloz, A. S., Elsner, J., Emanuel, K., & Henderson, N. (2015). Hurricanes and climate: The U.S. CLIVAR working group on hurricanes. *Bulletin of the American Meteorological Society*, *96*(6), 997–1017. https://doi.org/10.1175/BAMS-D-13-00242.1

Wan, H., Rasch, P. J., Taylor, M. A., & Jablonowski, C. (2015). Short-term time step convergence in a climate model. *Journal of Advances in Modeling Earth Systems*, *7*(1), 215–225. https://doi.org/10.1002/2014MS000368

Wan, H., Rasch, P. J., Zhang, K., Qian, Y., Yan, H., & Zhao, C. (2014). Short ensembles: An efficient method for discerning climate-relevant sensitivities in atmospheric general circulation models. *Geoscientific Model Development*, *7*(5), 1961–1977. https://doi.org/10.5194/gmd-7-1961-2014

Wan, H., Zhang, S., Rasch, P. J., Larson, V. E., Zeng, X., & Yan, H. (2021). Quantifying and attributing time step sensitivities in present-day climate simulations conducted with EAMv1. *Geoscientific Model Development*, *14*(4), 1921–1948. https://doi.org/10.5194/gmd-14-1921-2021

Webster, P. J., Holland, G. J., Curry, J. A., & Chang, H.-R. (2005). Changes in tropical cyclone number, duration, and intensity in a warming environment. *Science*, *309*(5742), 1844–1846. https://doi.org/10.1126/science.1116448

Wehner, M. F., Reed, K. A., Li, F., PrabhatBacmeister, J., Chen, C.-T., & Jablonowski, C. (2014). The effect of horizontal resolution on simulation quality in the Community Atmospheric Model, CAM5.1. *Journal of Advances in Modeling Earth Systems*. *6*(4). https://doi.org/10.1002/2013MS000276

Wieringa, J. (1992). Updating the Davenport roughness classification. *Journal of Wind Engineering and Industrial Aerodynamics*, *41*(1–3), 357–368. https://doi.org/10.1016/0167-6105(92)90434-C

Williamson, D. L. (2002). Time-split versus process-split coupling of parameterizations and dynamical core. *Monthly Weather Review*, *130*(8), 2024–2041. https://doi.org/10.1175/1520-0493(2002)130<2024:tsvpsc>2.0.co;2

Williamson, D. L. (2008). Convergence of aqua-planet simulations with increasing resolution in the Community Atmospheric model, version 3. *Tellus A: Dynamic Meteorology and Oceanography*, *60*(5), 848–862. https://doi.org/10.1111/j.1600-0870.2008.00339.x

Williamson, D. L. (2013). The effect of time steps and time-scales on parametrization suites. *Quarterly Journal of the Royal Meteorological Society*, *139*(671), 548–560. https://doi.org/10.1002/qj.1992

Williamson, D. L., & Olson, J. G. (2003). Dependence of aqua-planet simulations on time step. *Quarterly Journal of the Royal Meteorological Society*, *129*(591), 2049–2064. https://doi.org/10.1256/qj.02.62

Xie, S., Lin, W., Rasch, P. J., Ma, P.-L., Neale, R., Larson, V. E., et al. (2018). Understanding cloud and convective characteristics in version 1 of the E3SM Atmosphere Model. *Journal of Advances in Modeling Earth Systems*, *10*(10), 2618–2644. https://doi.org/10.1029/2018ms001350

Yu, S., & Pritchard, M. S. (2015). The effect of large-scale model time step and multiscale coupling frequency on cloud climatology, vertical structure, and rainfall extremes in a superparameterized GCM. *Journal of Advances in Modeling Earth Systems*, *7*(4), 1977–1996. https://doi.org/10.1002/2015MS000493

Zarzycki, C. M. (2016). Tropical cyclone intensity errors associated with lack of two-way ocean coupling in high-resolution global simulations. *Journal of Climate*, *29*(23), 8589–8610. https://doi.org/10.1175/JCLI-D-16-0273.1

Zarzycki, C. M., & Jablonowski, C. (2014). A multidecadal simulation of Atlantic tropical cyclones using a variable-resolution global atmospheric general circulation model. *Journal of Advances in Modeling Earth Systems*, *6*(3), 805–828. https://doi.org/10.1002/2014MS000352

Zarzycki, C. M., Levy, M. N., Jablonowski, C., Overfelt, J. R., Taylor, M. A., & Ullrich, P. A. (2014). Aquaplanet experiments using CAM's variable-resolution dynamical core. *Journal of Climate*, *27*(14), 5481–5503. https://doi.org/10.1175/JCLI-D-14-00004.1

Zarzycki, C. M., Reed, K. A., Bacmeister, J. T., Craig, A. P., Bates, S. C., & Rosenbloom, N. A. (2016). Impact of surface coupling grids on tropical cyclone extremes in high-resolution atmospheric simulations. *Geoscientific Model Development*, *9*(2), 779–788. https://doi.org/10.5194/gmd-9-779-2016

Zarzycki, C. M., Thatcher, D. R., & Jablonowski, C. (2017). Objective tropical cyclone extratropical transition detection in high-resolution reanalysis and climate model data. *Journal of Advances in Modeling Earth Systems*, *9*(1), 130–148. https://doi.org/10.1002/2016MS000775

Zarzycki, C. M., & Ullrich, P. A. (2017). Assessing sensitivities in algorithmic detection of tropical cyclones in climate data. *Geophysical Research Letters*, *44*(2), 1141–1149. https://doi.org/10.1002/2016GL071606

Zarzycki, C. M., Ullrich, P. A., & Reed, K. A. (2021). Metrics for evaluating tropical cyclones in climate data. *Journal of Applied Meteorology and Climatology*, *60*(5), 643–660. https://doi.org/10.1175/JAMC-D-20-0149.1

Zhang, G. J., & McFarlane, N. A. (1995). Sensitivity of climate simulations to the parameterization of cumulus convection in the Canadian Climate Centre general circulation model. *Atmosphere-Ocean*, *33*(3), 407–446. https://doi.org/10.1080/07055900.1995.9649539

Zhao, M., & Held, I. M. (2012). TC-permitting GCM simulations of hurricane frequency response to sea surface temperature anomalies projected for the late-twenty-first century. *Journal of Climate*, *25*(8), 2995–3009. https://doi.org/10.1175/JCLI-D-11-00313.1

Zhao, M., Held, I. M., & Lin, S.-J. (2012). Some counterintuitive dependencies of tropical cyclone frequency on parameters in a GCM. *Journal of the Atmospheric Sciences*, *69*(7), 2272–2283. https://doi.org/10.1175/JAS-D-11-0238.1